AD-A082 801 KAMAN SCIENCES CORP COLORADO SPRINGS COLO F/G 17/1
NOISE CANCELLATION TRANSDUCER DEVELOPMENT PROGRAM.(U)
MAY 79 V D PECKHAM, R T WINNICKI DNA001-77-C-0110
UNCLASSIFIED K-79-38 DNA-5048F NL

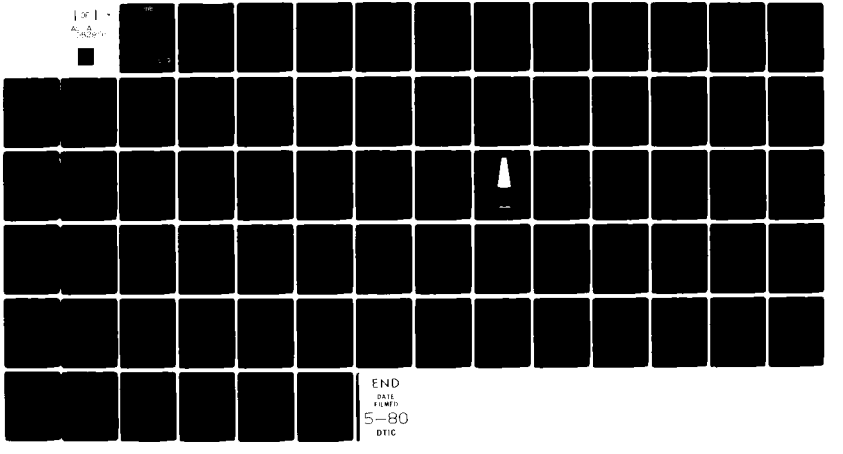

END
DATE FILMED
5-80
DTIC

(12) LEVEL III

AD-E 300 700

DNA 5048F

NOISE CANCELLATION TRANSDUCER DEVELOPMENT PROGRAM

Kaman Sciences Corporation
P.O. Box 7463
Colorado Springs, Colorado 80933

31 May 1979

Final Report for Period January 1977—May 1979

CONTRACT No. DNA 001-77-C-0110

THIS WORK SPONSORED BY THE DEFENSE NUCLEAR AGENCY
UNDER RDT&E RMSS CODE B342077464 N99QAXAA11212 H2590D.

Prepared for
Director
DEFENSE NUCLEAR AGENCY
Washington, D. C. 20305

Destroy this report when it is no longer needed. Do not return to sender.

PLEASE NOTIFY THE DEFENSE NUCLEAR AGENCY, ATTN: STTI, WASHINGTON, D.C. 20305, IF YOUR ADDRESS IS INCORRECT, IF YOU WISH TO BE DELETED FROM THE DISTRIBUTION LIST, OR IF THE ADDRESSEE IS NO LONGER EMPLOYED BY YOUR ORGANIZATION.

UNCLASSIFIED

SECURITY CLASSIFICATION OF THIS PAGE *(When Data Entered)*

REPORT DOCUMENTATION PAGE		READ INSTRUCTIONS BEFORE COMPLETING FORM
1. REPORT NUMBER DNA 5048F	2. GOVT ACCESSION NO.	3. RECIPIENT'S CATALOG NUMBER
4. TITLE *(and Subtitle)* NOISE CANCELLATION TRANSDUCER DEVELOPMENT PROGRAM		5. TYPE OF REPORT & PERIOD COVERED Final Report for Period January 1977–May 1979 6. PERFORMING ORG. REPORT NUMBER K-79-38
7. AUTHOR(s) Vernon D. Peckham Robert T. Winnicki		8. CONTRACT OR GRANT NUMBER(s) DNA 001-77-C-0110
9. PERFORMING ORGANIZATION NAME AND ADDRESS Kaman Sciences Corporation P.O. Box 7463 Colorado Springs, Colorado 80933		10. PROGRAM ELEMENT, PROJECT, TASK AREA & WORK UNIT NUMBERS Subtask N99QAXAA112-12
11. CONTROLLING OFFICE NAME AND ADDRESS Director Defense Nuclear Agency Washington, D.C. 20305		12. REPORT DATE 31 May 1979 13. NUMBER OF PAGES 74
14. MONITORING AGENCY NAME & ADDRESS*(if different from Controlling Office)*		15. SECURITY CLASS *(of this report)* UNCLASSIFIED 15a. DECLASSIFICATION DOWNGRADING SCHEDULE

16. DISTRIBUTION STATEMENT *(of this Report)*

Approved for public release; distribution unlimited.

17. DISTRIBUTION STATEMENT *(of the abstract entered in Block 20, if different from Report)*

18. SUPPLEMENTARY NOTES

This work sponsored by the Defense Nuclear Agency under RDT&E RMSS Code B342077464 N99QAXAA11212 H2590D.

19. KEY WORDS *(Continue on reverse side if necessary and identify by block number)*

Boundary Layer Transition
Wind Tunnel Testing
Noise Reduction
Spectrum Response

20 ABSTRACT *(Continue on reverse side if necessary and identify by block number)*

This report describes the development and ground testing of an acoustic sensor to detect boundary layer transition on models in high acoustic noise wind tunnel facilities. The noise cancellation transducer utilizes the Boundary Layer Acoustic Monitor (BLAM) detection concept to monitor the flow and employs a subtractive technique to cancel out coherent noise components to improve the signal to noise ratio.

DD FORM 1 JAN 73 1473 EDITION OF 1 NOV 65 IS OBSOLETE

UNCLASSIFIED

SECURITY CLASSIFICATION OF THIS PAGE *(When Data Entered)*

PREFACE

Kaman Sciences Corporation is submitting this report in partial fulfillment requirements of contrast DNA-001-77-C-0110. The work reported herein has been sponsored by Defense Nuclear Agency (DNA/SPAS) as part of the DNA Accuracy Program. Acknowledgements are especially given to Lcdr Richard Nibe, USN, Mr. Jimmy Dunn, PDA, and Dr. Anthony Demitriades, Ford Aerospace and Communications Corp. for their suggestions and help in the wind tunnel tests. Mr. T. Meagher was the KSC Program Manager for this program.

Conversion factors for U.S. customary to metric (SI) units of measurement.

To Convert From	To	Multiply By
angstrom	meters (m)	1.000 000 X E -10
atmosphere (normal)	kilo pascal (kPa)	1.013 25 X E +2
bar	kilo pascal (kPa)	1.000 000 X E +2
barn	meter^2 (m^2)	1.000 000 X E -28
British thermal unit (thermochemical)	joule (J)	1.054 350 X E +3
calorie (thermochemical)	joule (J)	4.184 000
cal (thermochemical)/cm^2	mega joule/m^2 (MJ/m^2)	4.184 000 X E -2
curie	*giga becquerel (GBq)	3.700 000 X E +1
degree (angle)	radian (rad)	1.745 329 X E -2
degree Fahrenheit	degree kelvin (K)	$t_K = (t°f + 459.67)/1.8$
electron volt	joule (J)	1.602 19 X E -19
erg	joule (J)	1.000 000 X E -7
erg/second	watt (W)	1.000 000 X E -7
foot	meter (m)	3.048 000 X E -1
foot-pound-force	joule (J)	1.355 818
gallon (U.S. liquid)	meter^3 (m^3)	3.785 412 X E -3
inch	meter (m)	2.540 000 X E -2
jerk	joule (J)	1.000 000 X E +9
joule/kilogram (J/kg) (radiation dose absorbed)	Gray (Gy)	1.000 000
kilotons	terajoules	4.183
kip (1000 lbf)	newton (N)	4.448 222 X E +3
kip/inch^2 (ksi)	kilo pascal (kPa)	6.894 757 X E +3
ktap	newton-second/m^2 ($N-s/m^2$)	1.000 000 X E +2
micron	meter (m)	1.000 000 X E -6
mil	meter (m)	2.540 000 X E -5
mile (international)	meter (m)	1.609 344 X E +3
ounce	kilogram (kg)	2.834 952 X E -2
pound-force (lbs avoirdupois)	newton (N)	4.448 222
pound-force inch	newton-meter (N·m)	1.129 848 X E -1
pound-force/inch	newton/meter (N/m)	1.751 268 X E +2
pound-force/foot^2	kilo pascal (kPa)	4.788 026 X E -2
pound-force/inch^2 (psi)	kilo pascal (kPa)	6.894 757
pound-mass (lbm avoirdupois)	kilogram (kg)	4.535 924 X E -1
pound-mass-foot^2 (moment of inertia)	kilogram-meter^2 ($kg·m^2$)	4.214 011 X E -2
pound-mass/foot^3	kilogram/meter^3 (kg/m^3)	1.601 846 X E +1
rad (radiation dose absorbed)	**Gray (Gy)	1.000 000 X E -2
roentgen	coulomb/kilogram (C/kg)	2.579 760 X E -4
shake	second (s)	1.000 000 X E -8
slug	kilogram (kg)	1.459 390 X E +1
torr (mm Hg, 0° C)	kilo pascal (kPa)	1.333 22 X E -1

*The becquerel (Bq) is the SI unit of radioactivity; 1 Bq = 1 event/s.
**The Gray (Gy) is the SI unit of absorbed radiation.

A more complete listing of conversions may be found in "Metric Practice Guide E 380-74," American Society for Testing and Materials.

TABLE OF CONTENTS

LIST OF FIGURES

LIST OF FIGURES (con't)

LIST OF TABLES

1.0 SUMMARY

The Noise Cancellation Transducer (NCT) program had as its objective, the development and test of a new transducer concept intended to permit the measurement of boundary layer signals in the presence of high background noise. Previous experience with the acoustic measurement of boundary layer signals in wind tunnels with the Boundary Layer Acoustic Monitor (BLAM) sensor have indicated that low signal to noise ratios (S/N ~1) results have been obtained due to the high background acoustic noise occuring in the wind tunnels.

A proposed NCT concept was designed, developed and tested, and the program work is described in this report. The design efforts included electronic circuitry as well as the prototype NCT, laboratory test methods and development of NCT's. These development efforts are described in Section 3.0. Some interesting data were obtained on a conical model in AEDC Tunnel B which suggests that the acoustic boundary layer signal is capable of offering a much more definitive understanding of boundary layer phenomena than data from other techniques. A test was also conducted in a small Mach 3 facility which provided data to verify that the NCT principles were indeed valid. Conclusions and recommendations are given in Section 4.0.

2.0 CONCEPT AND DEVELOPMENT

2.1 NCT Concept

The NCT was conceived as a result of experience with the (BLAM) in wind tunnel tests wherein it was observed that background tunnel noise obscured the boundary layer acoustic signal.[1] In studying the problem, differences in the character of the two signal sources were noted which could possibly be used for signal-to-noise improvement. Both the noise and signal sources at the point of origin are random spatially and temporily and thus nominally indistinguishable. The noise from the tunnel, however, is due primarily to a turbulent boundary layer on the nozzle wall and propagates some distance prior to incidence on the test model. Because the wave from a small area noise on the tunnel wall propagates spherically, the wave front is spatially coherent over a relatively large area at the model surface. On the other hand, the area over which the boundary layer signal on the model is coherent is small. Thus if a transducer were arranged such that the undesired spatially coherent components of a detected signal were suppressed then the non-coherent desired signal components could be more easily measured.

A transducer configuration is shown in Figure 1 which offers the potential for meeting the requirements stated in the preceding paragraph. In this configuration, two detectors are placed a short distance apart on the protected inside surface of the wind tunnel model. The outputs from the detectors are subtracted in a wideband difference amplifier and the output of the amplifier is processed as if it were a single BLAM sensor.

The separation of the two detectors depicted in Figure 1 is a critical factor in the noise cancellation technique. The cancellation of background noise is not as good with greater separation, however, the desired signal reception is improved by greater separation. Thus a trade off is required which depends on the boundary layer signal characteristics as well as the frequencies at which operation is desired.

The model wall pressure fluctuations are caused by corresponding boundary layer phenomena which have been investigated by a number of researchers who have measured pertinent boundary layer parameters including frequency content, r.m.s. pressure levels, turbulence pattern decay, correlation lengths etc.[2-7] In these references data were included which indicates that pressure fluctuations are statistically uncorrelated (phase incoherent) in distances comparable to the boundary layer velocity thickness δ. Reference 6 included the data presented graphically in Figure 2 illustrating that correlation in directions lateral and parallel to the flow. This figure shows that the boundary layer signals become uncorrelated in a shorter distance in the lateral direction than in the parallel direction.

These data indicate that at a sufficient separation distance the signal is uncorrelated and only minimally reduced when subtracted in the sensor pair. On the other hand, as the separation distance is increased the unwanted noise from the tunnel wall will tend to decorrelate on the model surface and subtraction will not result in a complete cancellation. The subtracted difference voltage (ΔV) characteristics out of the sensor pair is then dependent on the normalized correlation coefficients for the signal and noise (ρn, ρs) and the difference voltage may be given as:

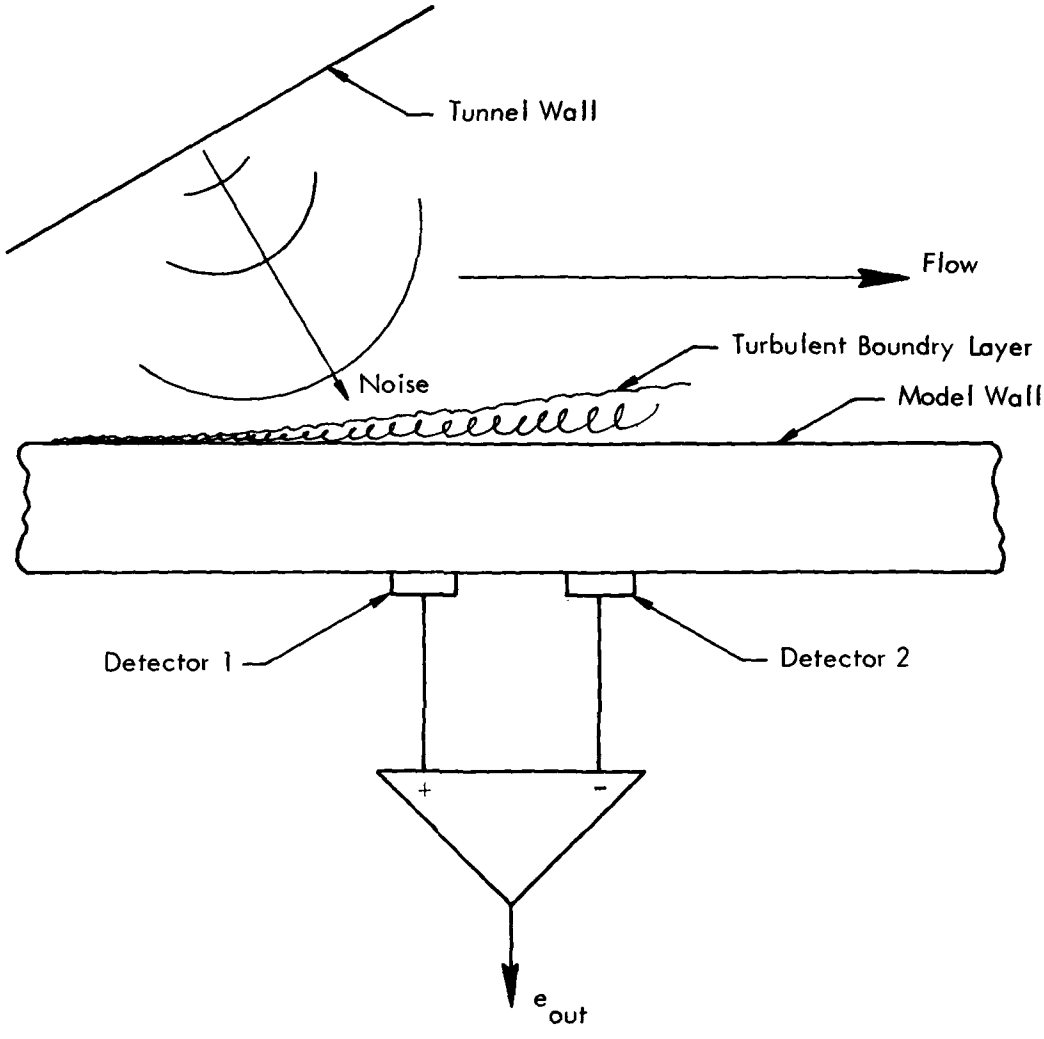

Figure 1. NCT Configuration

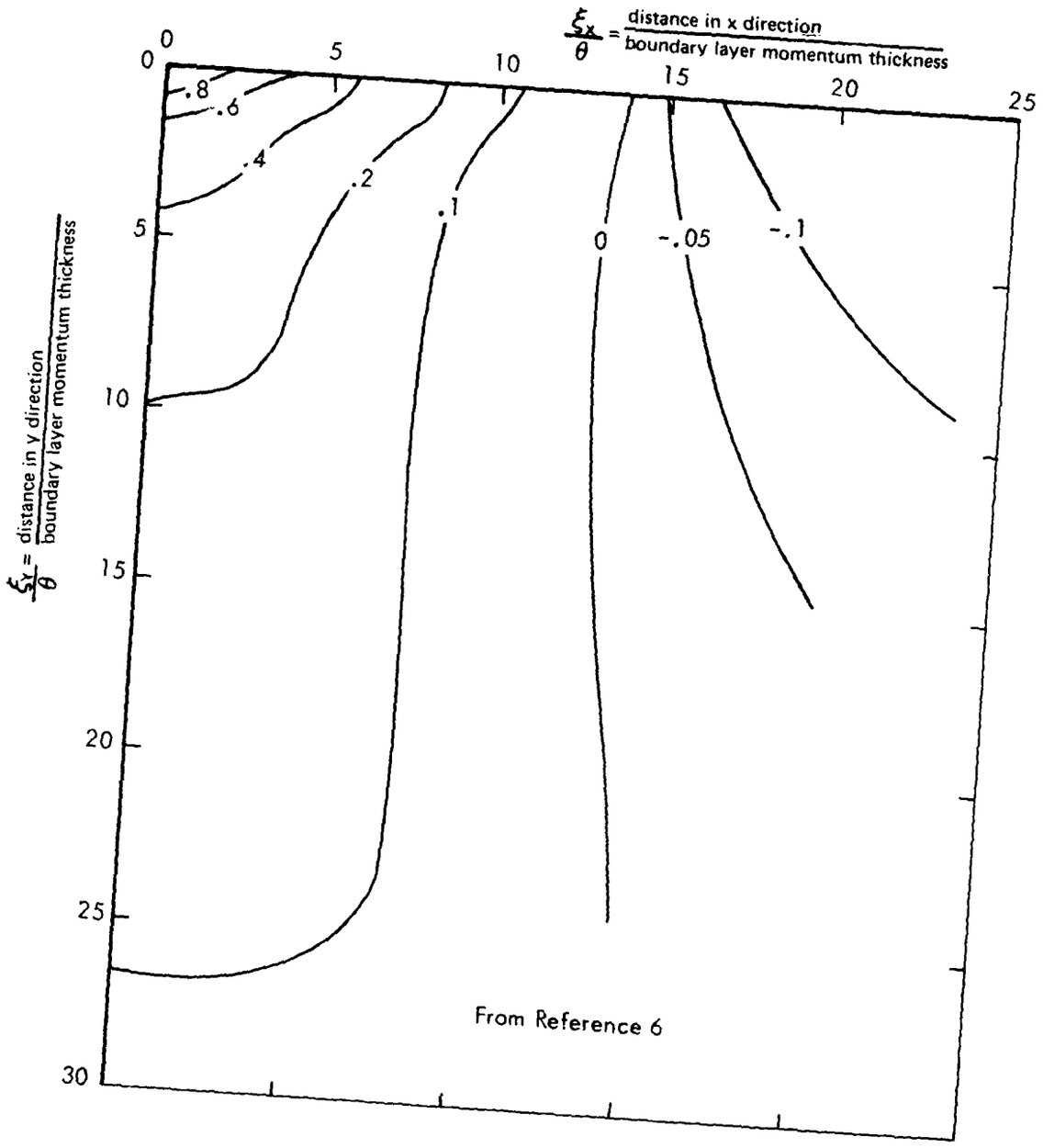

Figure 2. Approximate Contours of Equal Correlation Coefficient in Unperturbed Flow, $M = 3.45$

$$V = \left(2V_s^2(1-\rho s) + 2V_n^2(1-\rho n)\right)^{1/2}$$

where:

V_s = Voltage component from one sensor due to signal

V_n = Voltage component from one sensor due to noise

ρ_s = Normalized correlation coefficient for signal

ρ_n = Normalized correlation coefficient for noise

The signal to noise ratio for the difference voltage output is:

$$(S/N)_\Delta = \frac{V_s}{V_n}\left(\frac{1-\rho s}{1-\rho n}\right)^{1/2}$$

and this can be larger than the signal to noise ratio from a signal sensor (V_s/V_n) depending upon the values of the signal and noise correlations.

The exact nature of signal and noise propagation from the model surface to the sensors imbedded in the model heatshield requires numerical solution techniques beyond the scope of this program. It is apparent that heatshield/sensor interactions, wave propagation in the heatshield and heatshield/sensor resonances will affect both the signal and noise correlations and will also affect the NCT signal to noise performance improvement. The approach to developing a workable NCT boundary layer sensor on this program has relied primarily on laboratory developments and empirical tests to provide a NCT to be evaluated in controlled wind tunnel tests. The NCT development and wind tunnel tests conducted on this program are discussed in the following sections.

2.2 Prototype Development

The NCT prototype design is depicted in Figure 3. Two small crystals were placed side by side on a thin aluminum plate with opposite polarity orientation as noted in the Figure. The circuit shown includes two preamplifiers to buffer the high impedance of the crystal to the lower impedance of the balancing or "null" potentiometer. The single-ended output is then amplified and conditioned by additional circuitry.

To measure the performance of the prototype NCT in the laboratory a jet of air flowing from a small orifice was used as a time-random noise source. While this technique produced a qualitative measure of the effective reduction of a spatially coherent noise source, the desired boundary layer signal could not be generated simultaneously. The wind tunnel itself appears to be the only technique for producing the unique conditions simultaneously.

The cancellation of air nozzle noise by the prototype NCT is shown in Figure 4 versus nozzle distance. This plot shows that there is a relatively weak dependence on distance. Frequencies accepted in the circuit in obtaining the data in Figure 4 ranged up to 400 khz. It was noticed that the cancellation was improved in certain frequency bands within the range of frequencies being used.

Using a narrow frequency band and smaller crystals produced better cancellation ratios in the laboratory, however, the ratios were still lower than desired. A careful examination of the data and spectrum analyzer displays showed that the plate on which the NCT was mounted was the greatest source producing uncorrelated components which were not cancelled out in the difference voltage output.

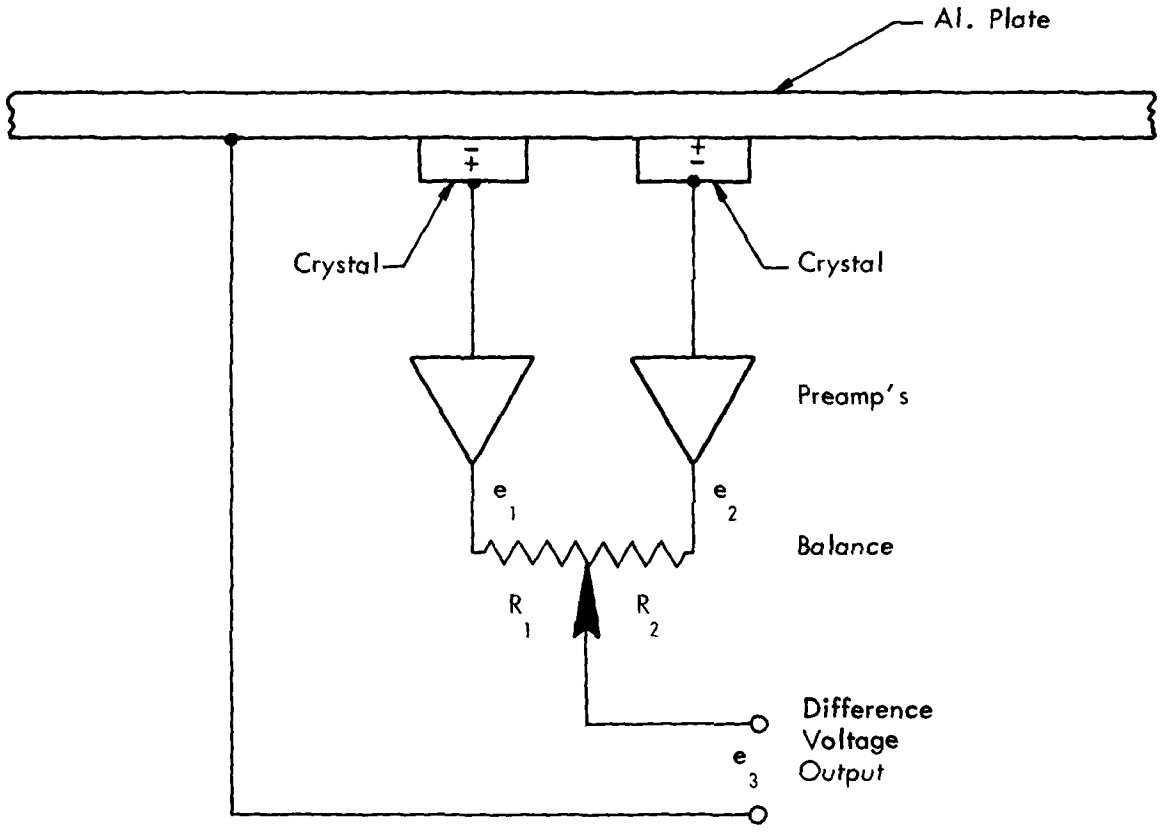

Figure 3. NCT Prototype

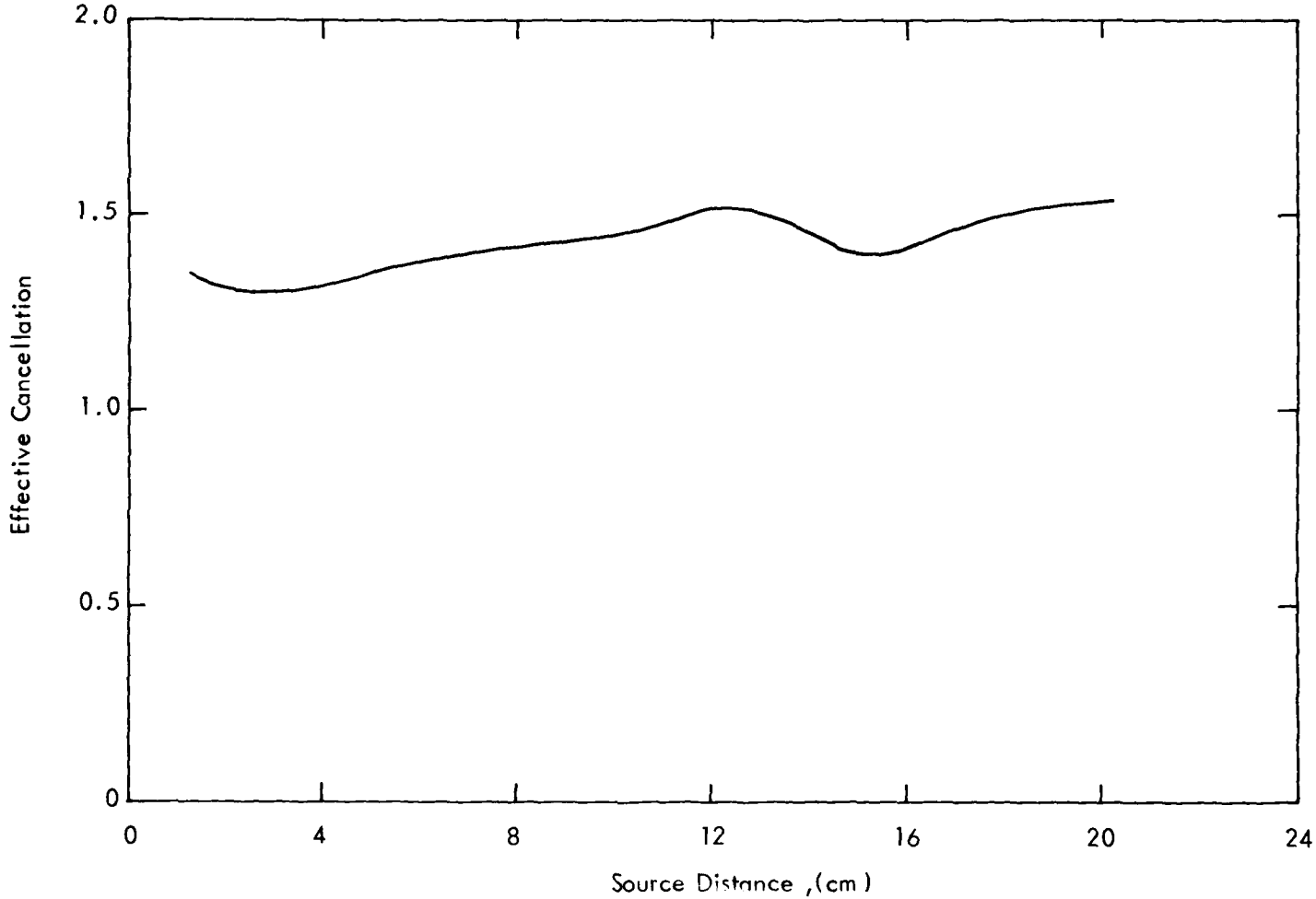

Figure 4. Effective Cancellation Ratio
(Air Nozzle Excitation)

The approach then turned to techniques to reduce the effect which resonances of the plate might have on the NCT performance. The result of this investigation was the development of a design similar to the final design configuration of the NCT, shown in Figure 5. Features of this design include a thin face plate on which the crystals are mounted and a heavy wall cylinder the purpose of which is to provide stiffening in the area of the sensors.

The prototype NCT was tested on several surfaces representing those which are found in wind tunnel models. The gage was mounted inside a 0.13 cm alumunium cone frustum, a 1 cm thick carbon phenolic (CP) cone and in a counterbored hole on the 1 cm CP cone. The configurations are sketched in Figure 5.

In terms of the air nozzle noise cancellation ratios were measured for the three installations as follows:

Configuration	Cancellation Ratio
0.13 cm Aluminum wall	4 to 6
1.0 cm CP	2 to 3
Counterbored 1.0 cm CP	8 to 12

It was noticed that the best cancellation ratio appeared to be in the 50 khz to 70 khz frequency band as indicated by a spectrum analyzer display of the sensor output.

In addition to the NCT sensors, a general purpose amplifier was designed which could be applied in the laboratory and to wind tunnel measurements. The circuit of this amplifier is shown in Figure 6; it is a linear FET amplifier with response

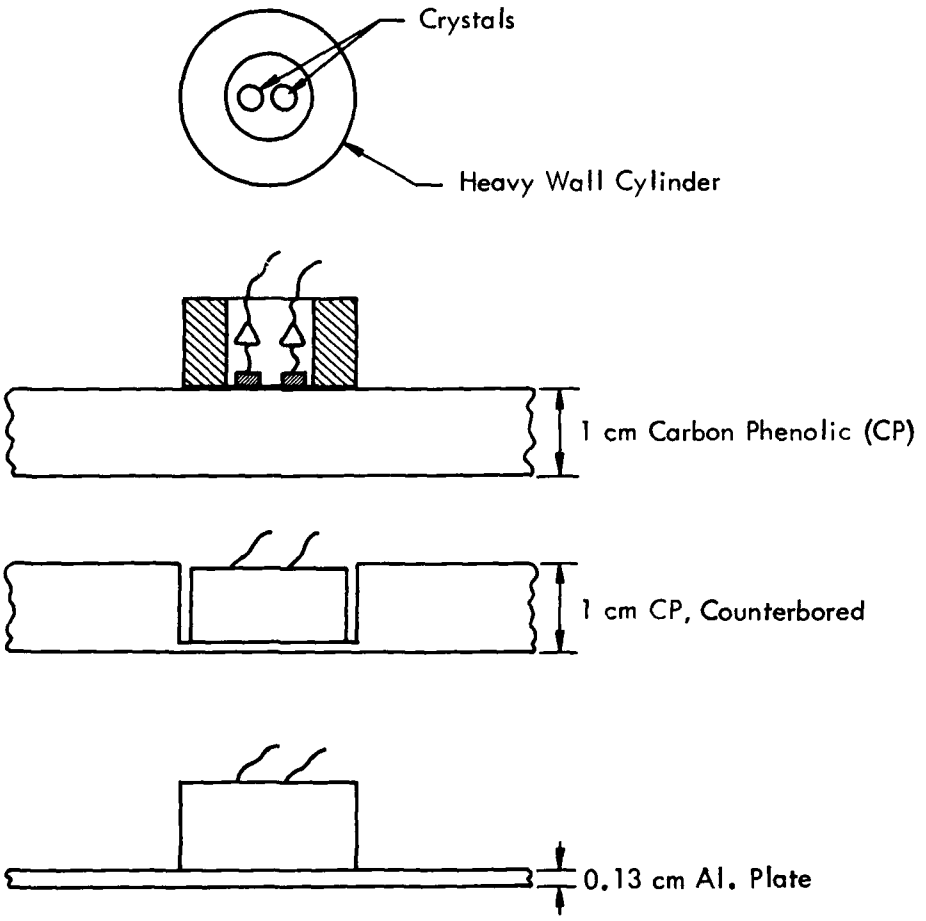

Figure 5. Development NCT Configuration

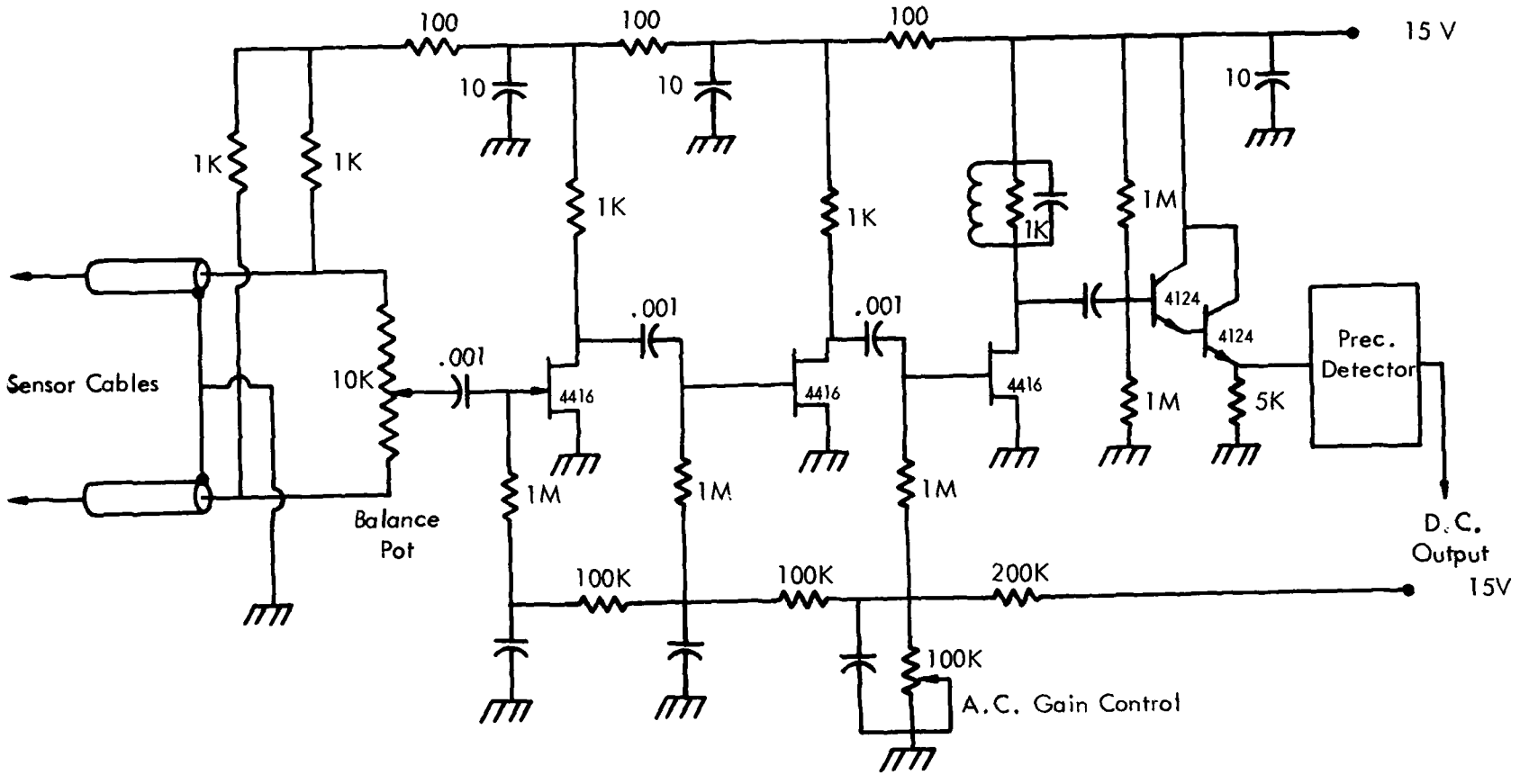

Figure 6 . NCT Breadboard Circuit

to over 1 MHz followed by a precision envelope detector. The output is a d.c. voltage proportional to the acoustic signal amplitude at the center arm of the balance potentiometer. The amplifier requires a balanced $\pm$15 volt power supply and can produce up to 10 volts at the output.

To summarize, the NCT sensor developed on this program consists of two reversed polarity PZT crystals contained in a heavy wall cylindrical housing. Based upon the laboratory air muzzle tests, the sensor spacings was selected to be approximately 2 mm. The counterbored CP heatshield installation with the NCT approximately 1 mm from the flow appeared to perform the best in the laboratory. The linear FET difference amplifier used with the precision envelope detector is the signal conditioner unit most applicable for NCT/wind tunnel testing.

3.0 GROUND EVALUATION TESTS

3.1 Small Model Wind Tunnel Test

To obtain an early verification of the NCT concept, a wind tunnel test was planned and carried out at the Ford Aerospace and Communication Corporation (FACC) Supersonic Wind Tunnel (SWT) in Newport Beach, California. The test objectives centered on obtaining data from the prototype NCT in an environment containing both signal and noise.

The SWT tunnel operating parameters are shown in Table 1.

Table 1
FACC/SWT Wind Tunnel Parameters

MACH 3
T_o = 38°C
P_o = 200 mm Hg to 730 mm Hg continuously variable
Reynolds No - 2.6 to 6.9 x 10^6/m.
Test Area - 8 cm x 12 cm

Due to the small tunnel size it was necessary to limit the base diameter of the model to approximately 2.5 cm. The model design and NCT locations are shown in Figure 7; it was machined out of a solid cylinder of stainless steel and had a cavity in the back in which the NCT's were installed. The wall thickness which separated the NCT from the flow was 1 mm.

Because the model was so small, the NCT's were constructed integrally into the model with no heavy wall cylinder. Some problems were experienced in controlling the effects of cone resonances but by potting the base cavity with epoxy, satisfactory damping was achieved. In the KSC laboratory, a cancellation ratio of 3:1 was observed with the air nozzle source.

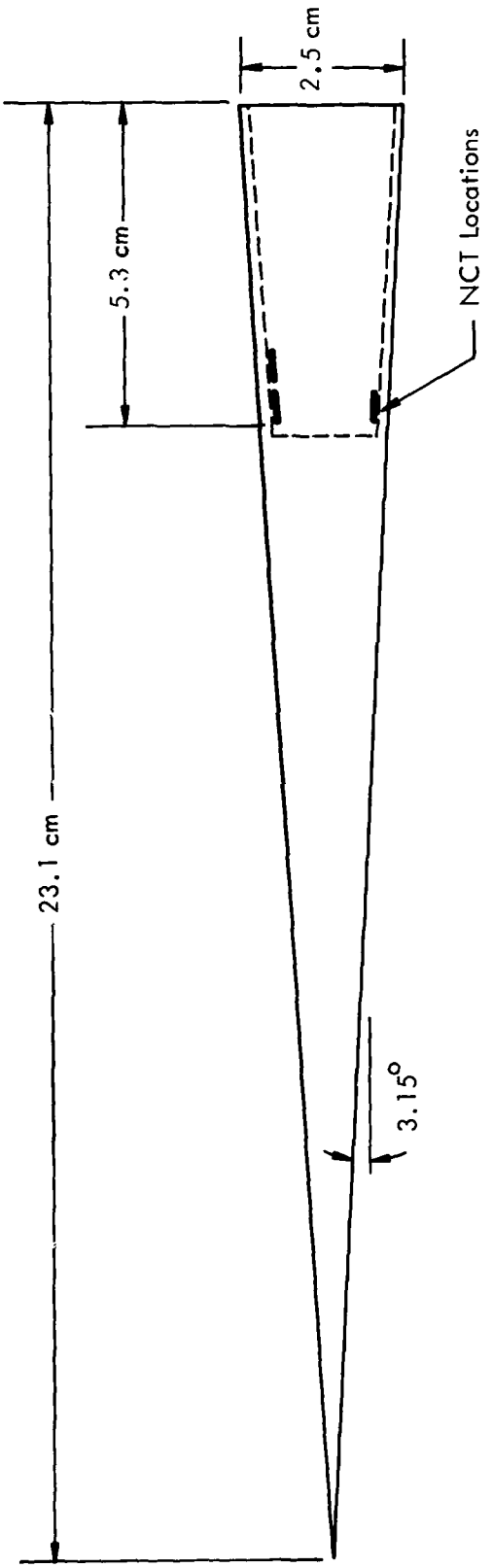

Figure 7. Small Wind Tunnel Model

As noted in Figure 7, the model was built with two NCT's, in one of which the two crystals were aligned parallel to the model axis and in the other the two crystals were aligned normal to the model axis. The purpose for this arrangement was that of providing a test of the NCT function which is based on the acoustic correlation length in the boundary layer. As indicated earlier, the cross-axis transducer was anticipated to function better than the parallel-axis transducer because correlation lengths are longer in the parallel-axis direction. (See Figure 2).

The wind tunnel experiment consisted of a series of runs in which the tunnel pressure (P_o) was varied uniformly to produce corresponding Reynolds number variations. Data at each Reynolds number were acquired via a digital volmeter and a spectrum analyzer which had response ranging up to 100 khz.

The signal from each crystal was brought out independently through a coaxial cable to the circuit shown in Figure 6; data were recorded on the spectrum analyzer from the filtered amplifier a.c. output taken off just before the precision rectifier or from the center arm of the balance potentiometer. All d.c. voltages recorded were at the output of the precision rectifier.

Examples of the d.c. voltage data obtained in this test are shown in Figures 8 through 11. Data in Figures 8 and 9 were taken over a tunnel pressure range of 350 to 730 mm Hg with no external transition trips on the model. Under these conditions turbulence did not occur over the NCT locations for the range of tunnel pressures and was observed to occur only at the aft end of the model at the 730 mm Hg pressures (Ref. 11). The data of Figures 8 and 9 do show an increase in output at the highest tunnel pressures

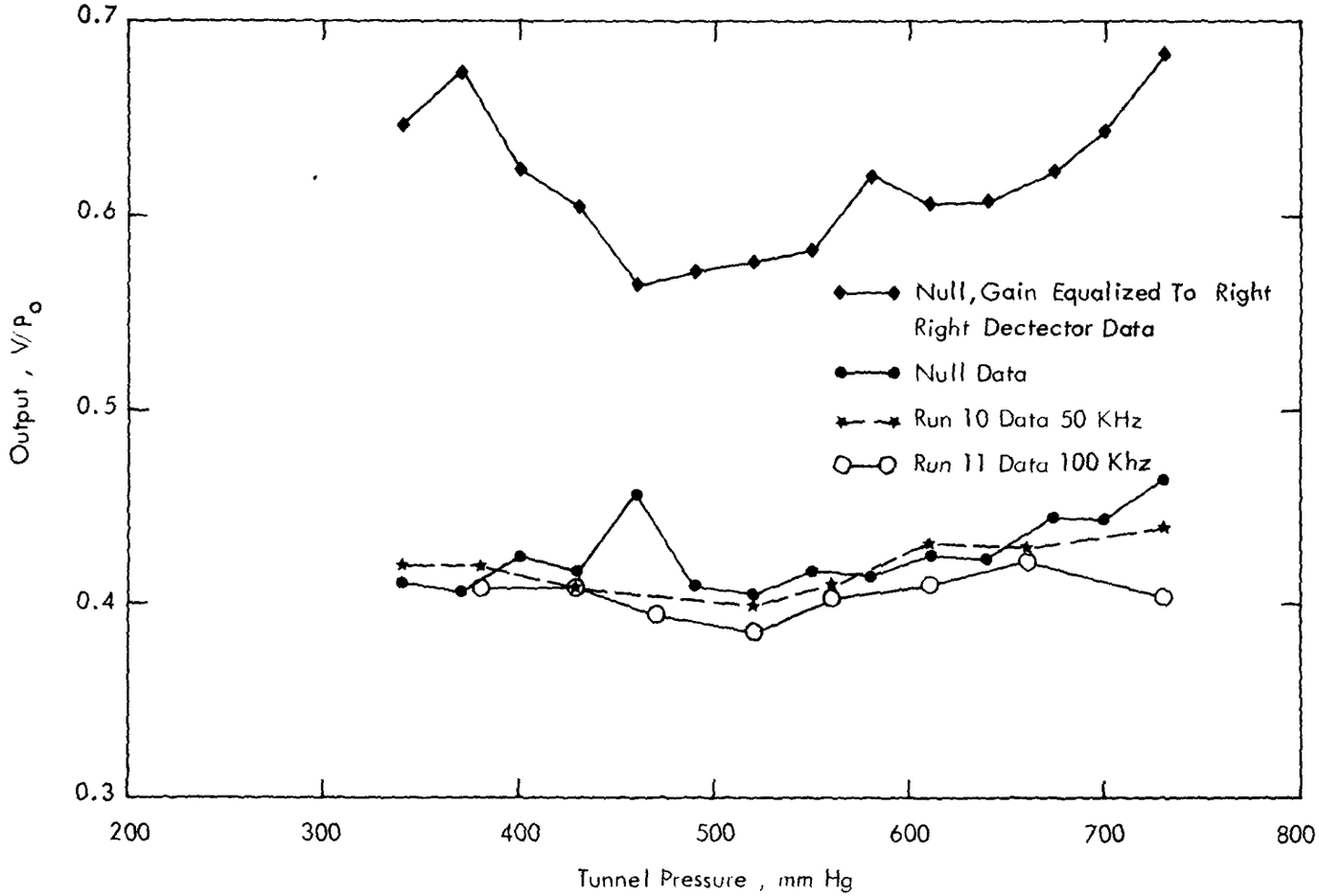

Figure 8. NCT Parallel to Flow (Run 1)

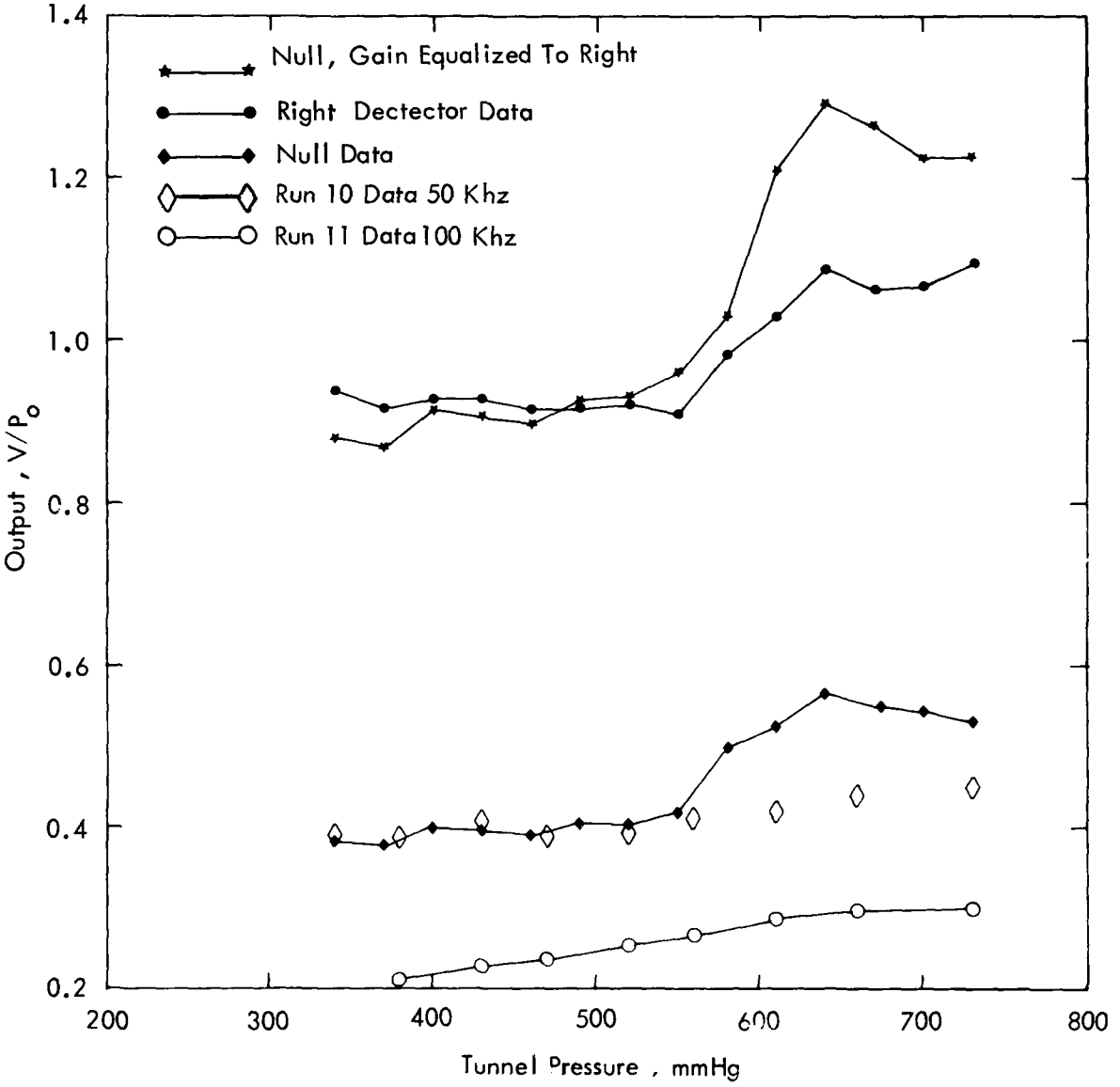

Figure 9 . NCT Normal to Flow (Run 2)

indicating that transition to turbulence is starting at the NCT locations. The data shown in Figures 10 and 11 were taken with an axisymmetric transition trip installed near the forward tip of the model which caused turbulence at the NCT locations. The three curves shown in each of these figures are the null position difference voltage outputs for three identical data sets and thus indicate the type of repeatability which was acheived. Transition is clearly observed in the cross flow NCT configuration shown in Figure 11 although it is not as distinct in the parallel flow NCT configuration data of Figure 10.

Additional information is shown in Figures 12 and 13 which are spectral plots of the cross-axis transducer output for tunnel pressures of 520 and 610 mm Hg. Figure 12 is a plot of filted a.c. amplifier output voltage and shows that at the frequency of the filter (50 khz), a distinct peak indicates transitions. The broadband data in Figure 12 show that only selected frequencies indicate transition. This broadband signal was obtained at the input of the amplifier at the balance potentiometer null output.

The results of the SWT wind tunnel test showed that even on this very small model, the NCT detected transition in the presence of a high background noise. The signal-to-noise ratio was improved for the cross flow configuration but not as greatly as hoped for perhaps because of model surface curvature.

3.2 AEDC Wind Tunnel Test

3.2.1 Test Summary Information

The primary purpose for conducting a wind tunnel test was that of proving that the NCT would function as postulated in a

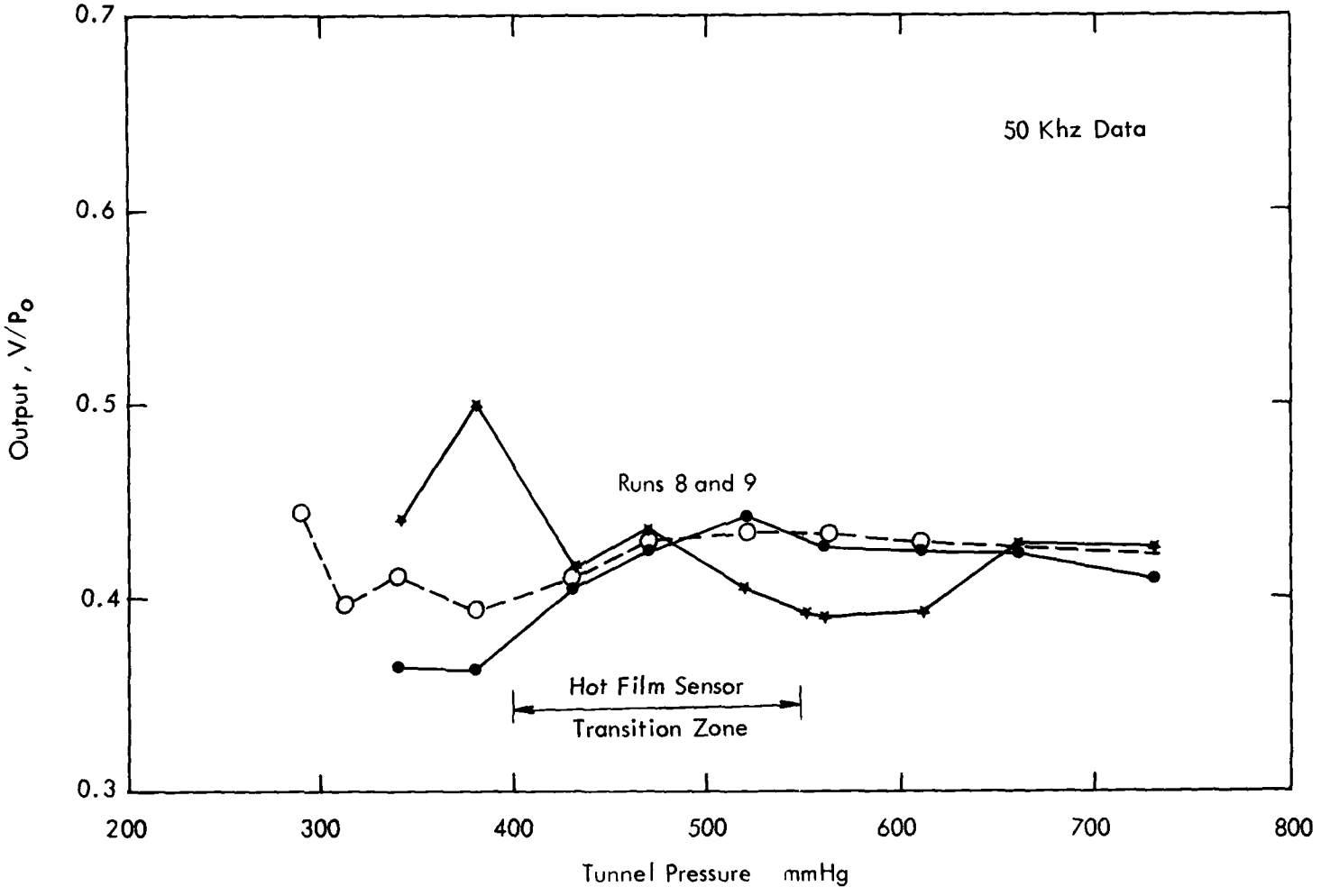

Figure 10 . NCT Parallel to Flow with Trip (Null Output)

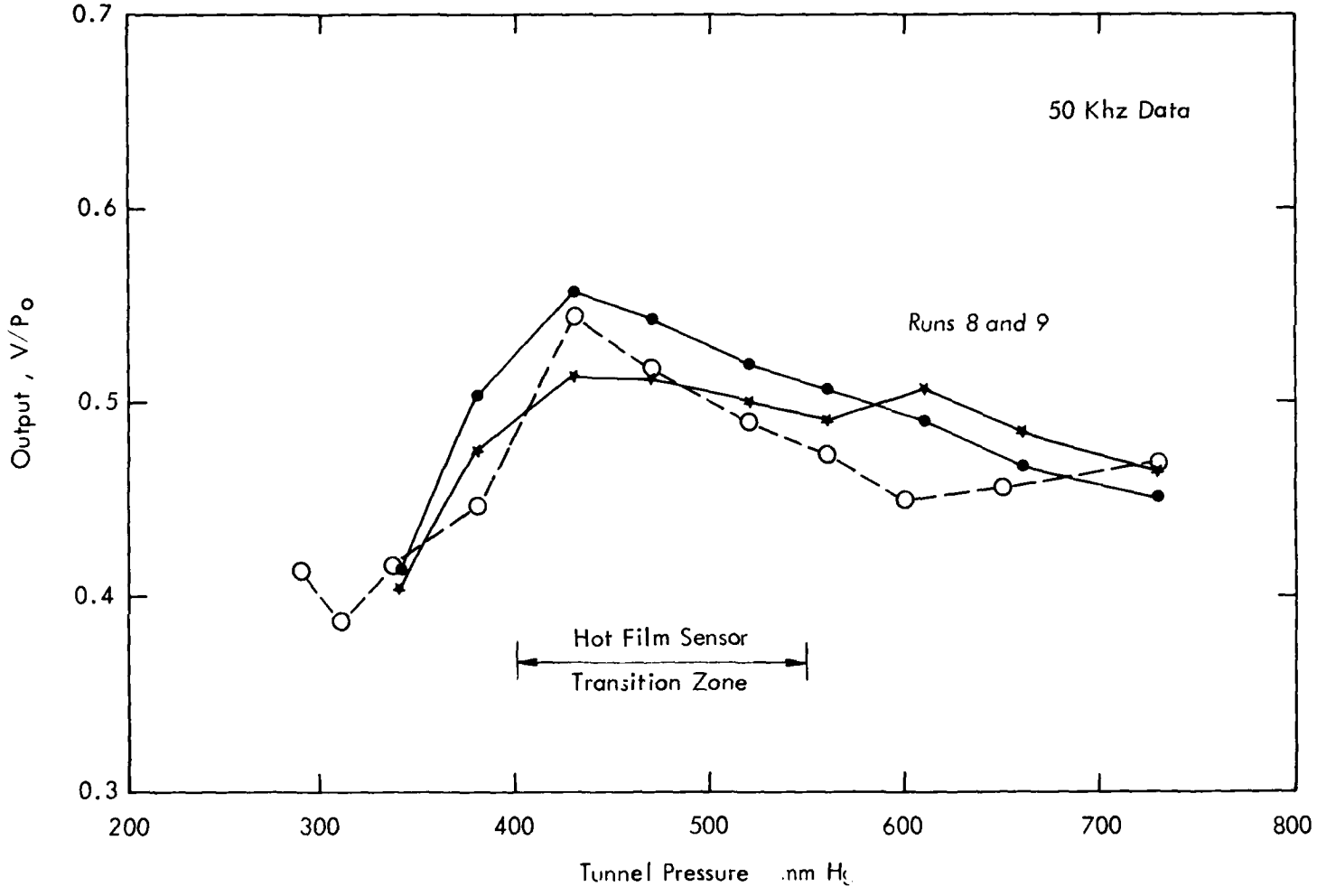

Figure 11. NCT Normal to Flow with Trip (Null Output)

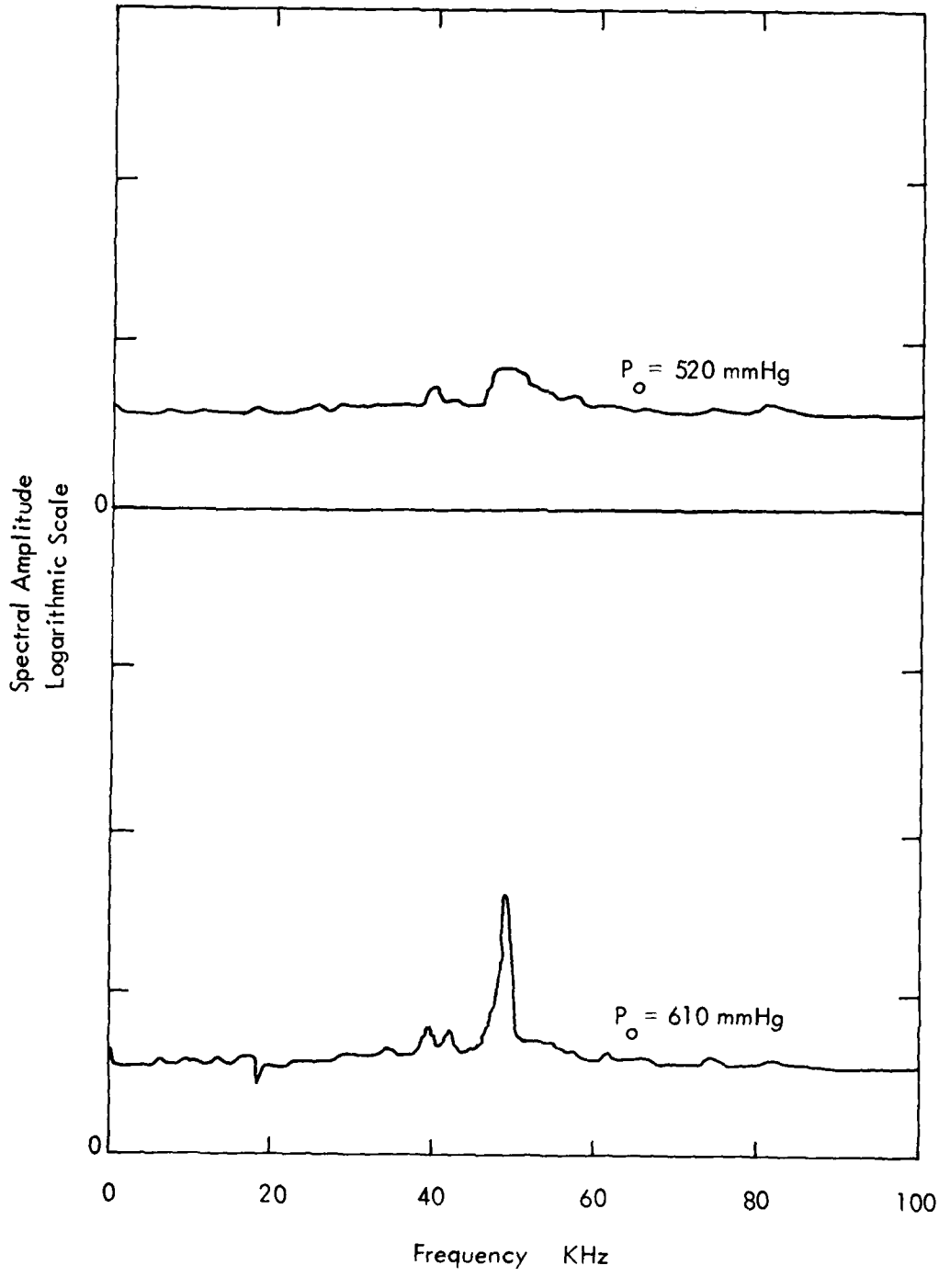

Figure 12. Cross Flow NCT Spectrum, Narrow Band (50 Khz Filter)

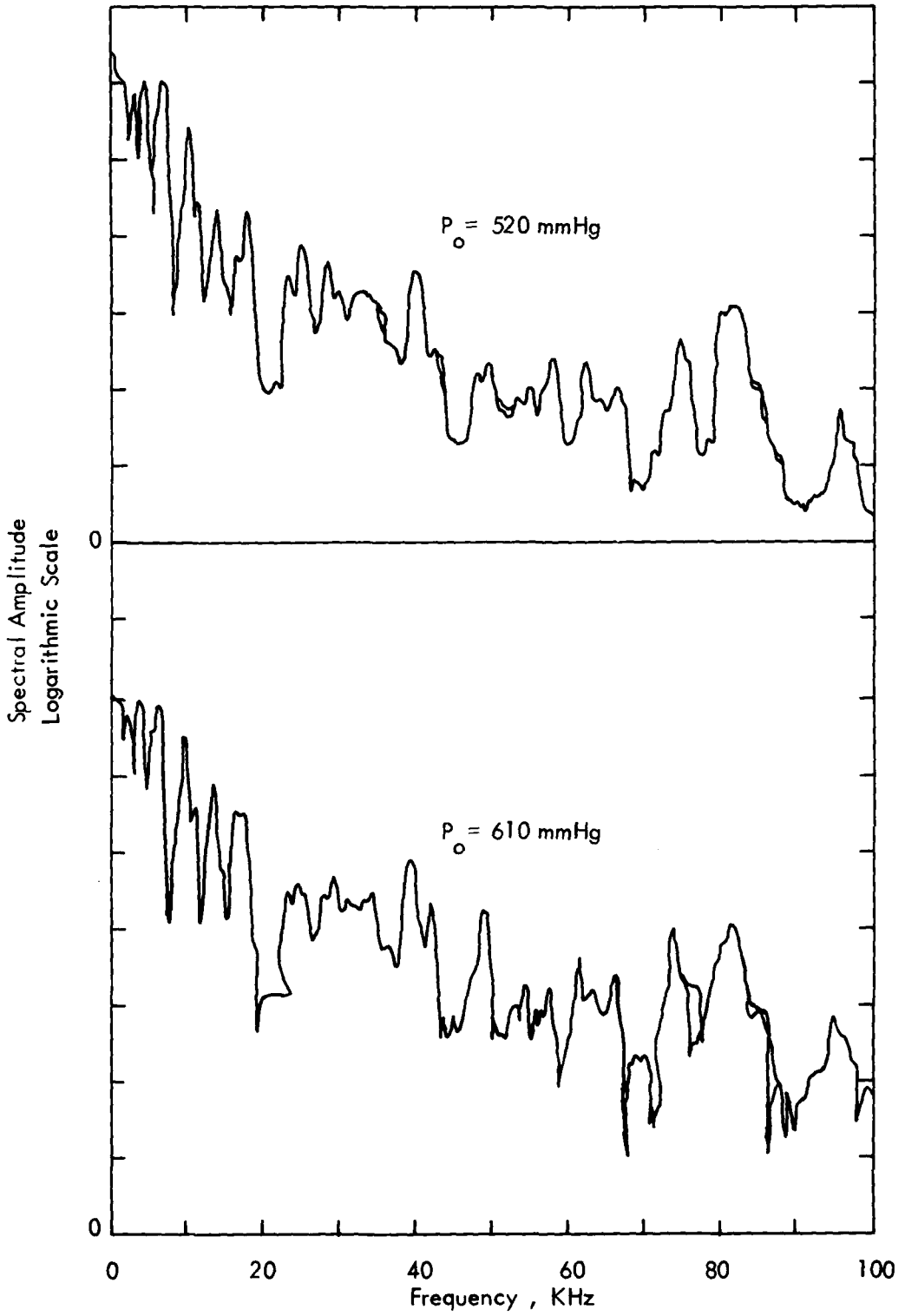

Figure 13. Cross Flow NCT Spectrum Broadband

noise environment. To accomplish this objective, a sharp conical model, on which were installed a number of NCT's was placed in hypersonic flow at varying Reynolds numbers. The Reynolds numbers in the wind tunnel were chosen such that both laminar and turbulent flow would be present on the model. The NCT, if functioning properly, would produce a signal with improved signal-to-noise ratio in response to the turbulent boundary layer.

At the request of DNA, the wind tunnel test was planned and implemented as a "piggyback" in conjunction with a series of on-going tests being conducted by another DNA prime contractor, Prototype Development Associates (PDA). The PDA program included entry into the AEDC Tunnel B at Mach 8 with a sharp nose model. Test parameters with a spinning model were as follows:

M_∞ = 8.0

Re_∞ = 3.6, 1.2, 0.6 million/meter

Spin rate = 0, 1, 2, 3 rps

Angle of attack = 0, 0.3, 0.6, 1.2, 1.8, 3.6°

Angle of attack sweep = -6° to +6° continuous

The test model design was based on the piggyback approach and included mechanical and electrical interfacing to the PDA model. KSC-furnished parts included a stainless steel nose-tip section, a carbon-phenolic mid section and an aluminum aft section. These parts were designed to interface with the PDA substructure which was mounted on the tunnel string.

Electrical interfacing was accomplished via miniature rectangular connectors which mated to PDA connectors inside the model shell. A photograph of the model is shown in Figure 14 and a layout sketch showing instrumentation is presented in Figure 15.

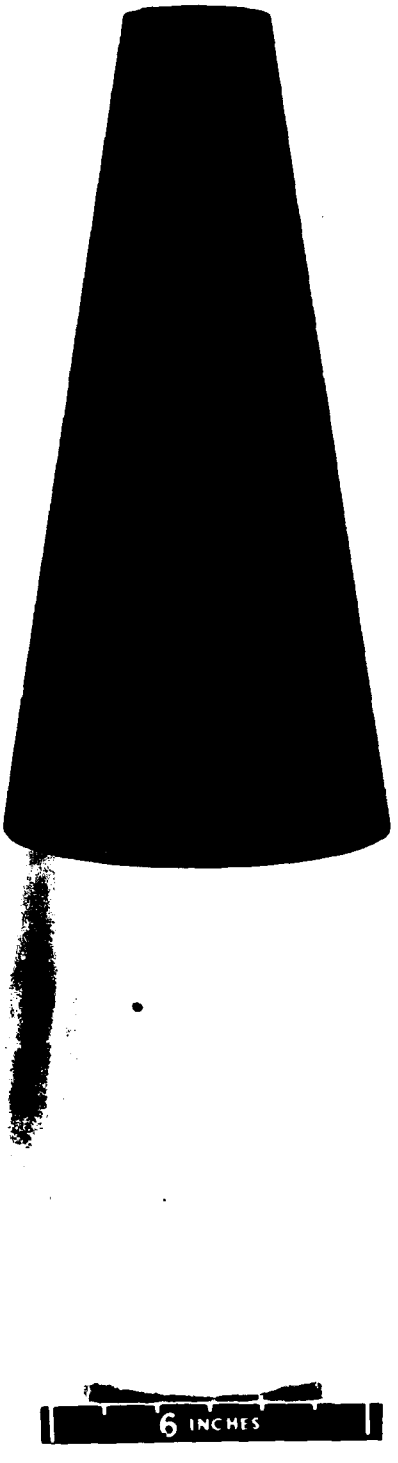

Figure 14. AEDC Wind Tunnel Test Model

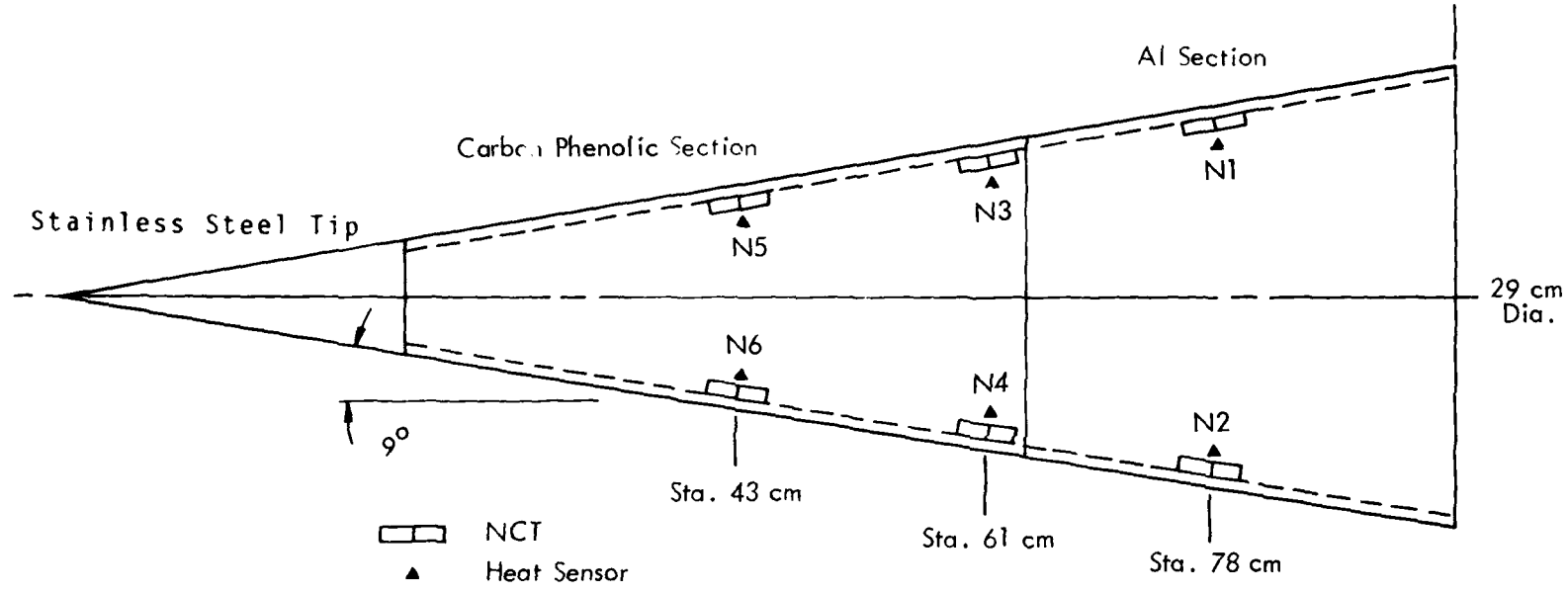

Figure 15. Model Instrumentation Layout

In addition to NCT's, fast response surface temperature thermocouples were installed in the model and are visible in the photograph of Figure 14 as the circular dots on the surface. These thermocouples were designed to be useful primarily for fairly rapid temperature change detection as is experienced on the surface of a rotating model at an angle of attack with intermittent laminar and turbulent flow at the thermocouple location.

Boundary layer transition on the model was expected to be similar to that measured by PDA with Gardon gages in identical flow condition. Representative PDA results are shown in Figures 16-20 for unit Reynolds number or 4×10^{-6} per meter. The shaded areas on the model show the measured locations of turbulence at angles of attack up to 6°. It can be noted that transition moves rapidly forward on the leeward ray at small angles of attack. If the model were rotating, a transducer at appropriate locations would pass through consecutive zones of laminar and turbulent flow.

The test plan as originally conceived included obtaining data with a rotating model but at test time the model bearings were inoperable. Static and angle-of-attack sweep data were obtained but not with a rolling model. The model was oriented so that at an angle of attack one array of transducers (Ref. Figure 15) was leeward and the other array was on the windward azimuth.

A total of 26 data groups was obtained during the allocated time; test conditions are shown in Table 2. Data from groups 1059 through 1078 qualified as useful test data and were analyzed to determine if test objectives were achieved.

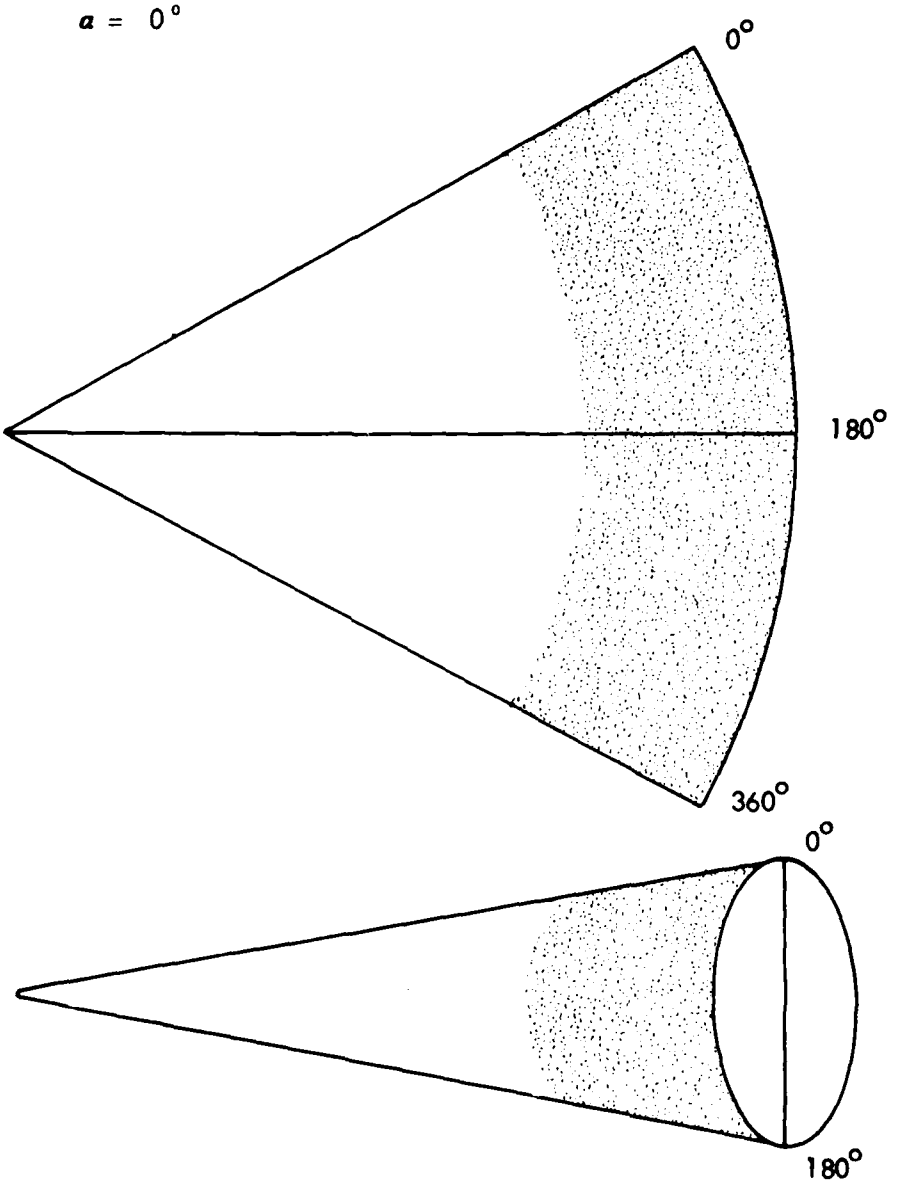

Figure 16. Transition On Cone (PDA Data)

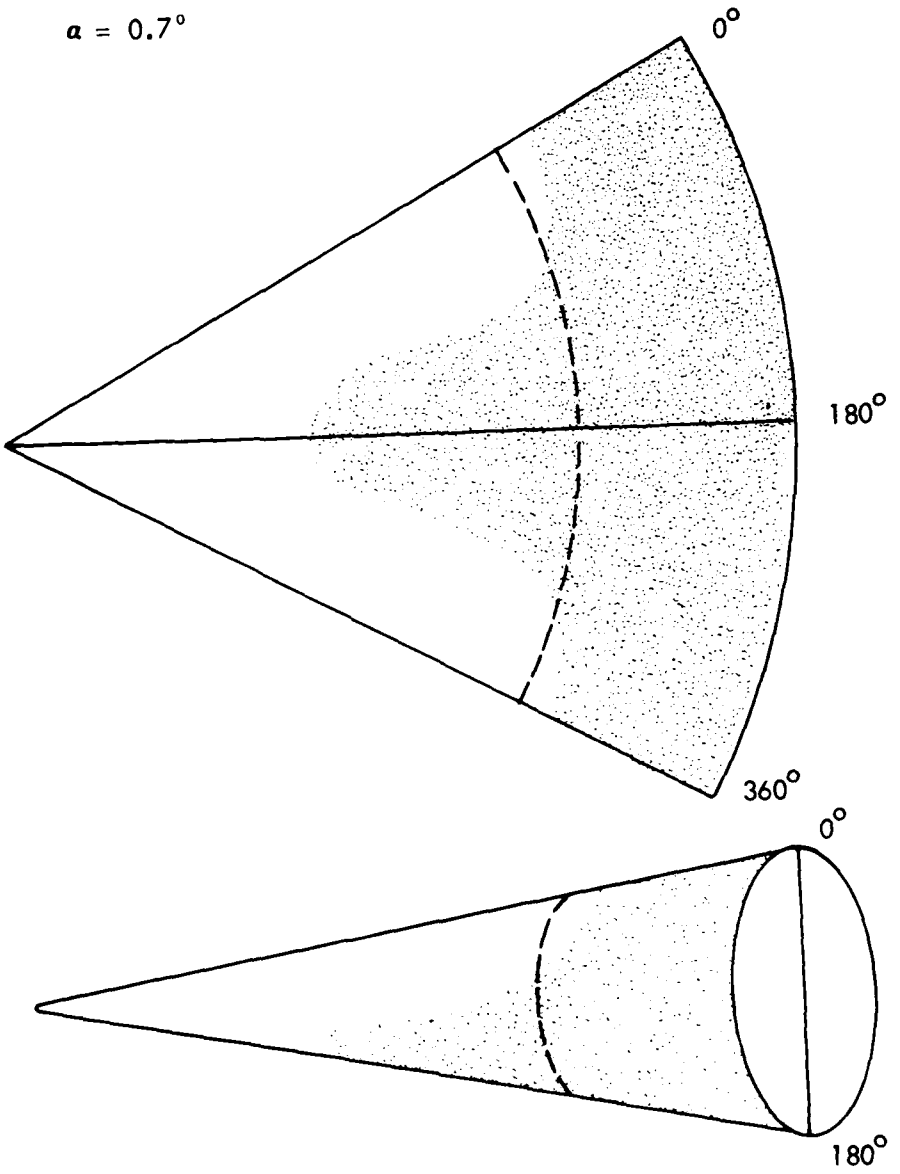

Figure 17. Transition On Cone (PDA Data)

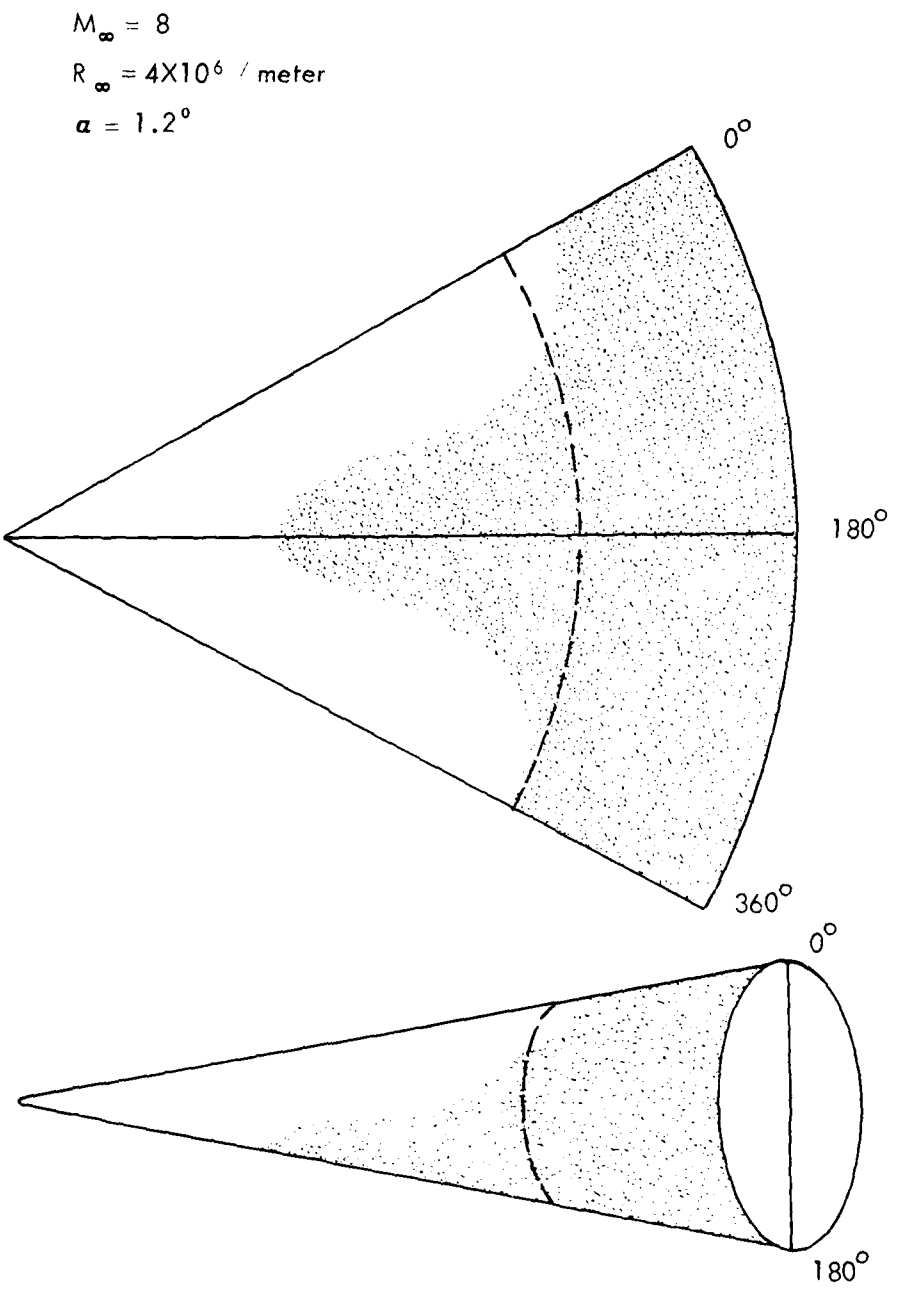

Figure 18. Transition On Cone (PDA Data)

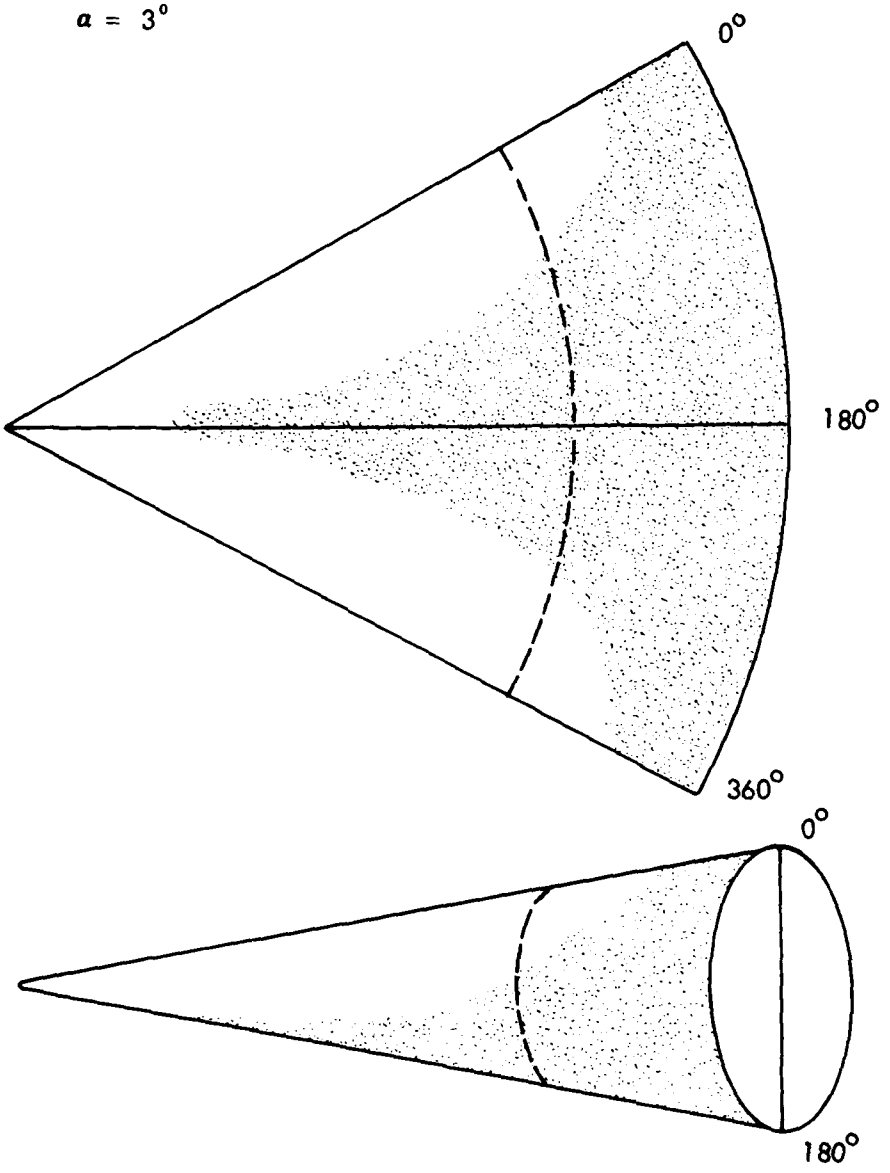

Figure 19. Transition On Cone (PDA Data)

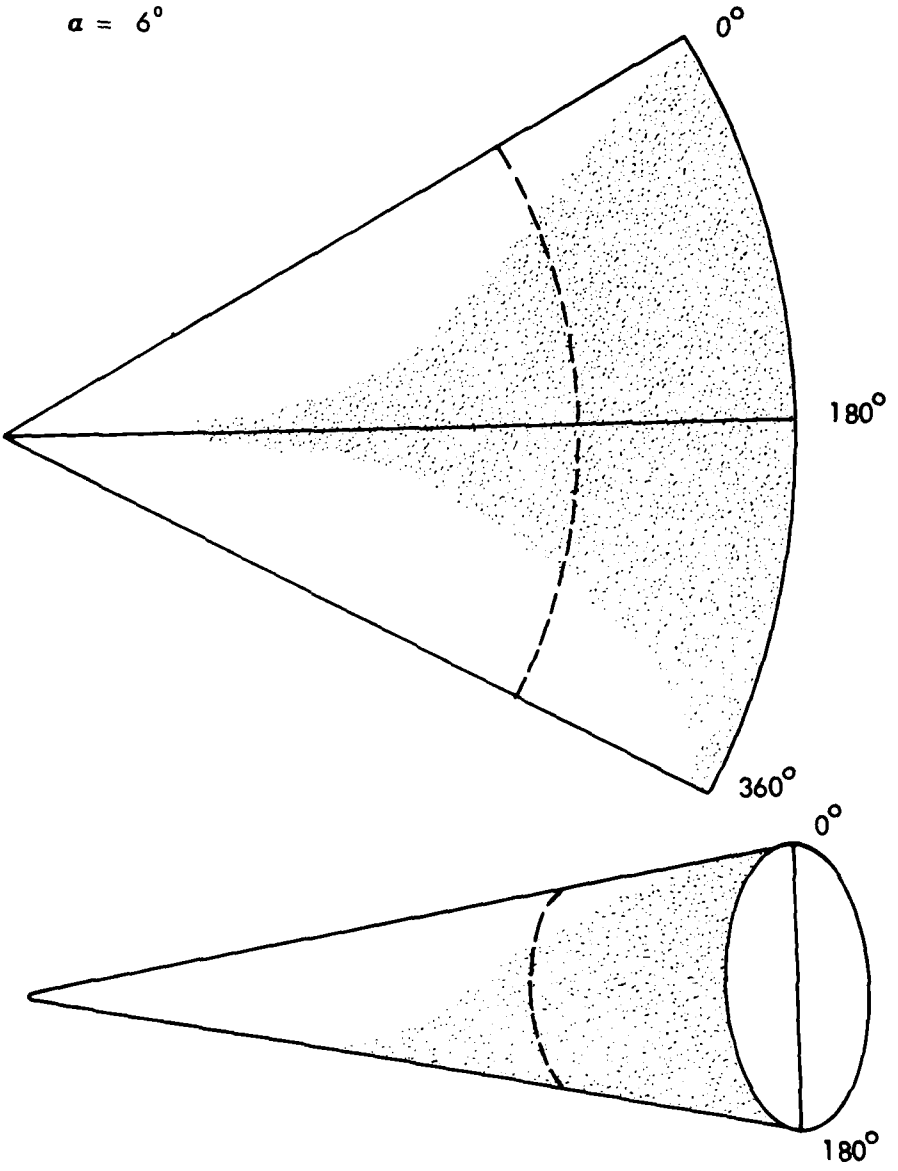

Figure 20. Transition On Cone (PDA Data)

Table 2

AEDC Wind Tunnel Test

Data Conditions

Group No.	R_∞	α(degrees)	NCT Settings
			Initial Null Search
1053	4×10^6/m	0	
1054			
1055			
1056			
1057			
1058			Null
1059		1.25	
1060		2.50	
1061		0	Right
1062		1.25	
1063		2.50	
1064		0	Left
1065		1.25	
1066		2.50	
1067		-6 to +6 Sweep	Null
1068			
1069	8×10^6/m	0	
1070		1.25	
1071		2.50	
1072		0	Right
1073		1.25	
1074		2.50	
1075		0	Left
1076		1.25	
1077		2.50	
1078		-6 to +6 Sweep	Null

Data were acquired in two forms: digital and analog. Digital data were obtained by the AEDC data system which samples transducer d.c. voltages, converts to digital form and records on magnetic tape. Broadband signals from the NCT balance potentiometer were recorded on a Bell and Howell 3700B analog tape recorder with a bandwidth to 500 khz.

3.2.2 Digital Data

Because the static model data are essentially non-varying during the data sampling period, the data are presented here in tabular form. Table 3 contains data for Re_∞ of 4 million/meter and Table 4 is a list of data for Re_∞ of 8 million/meter. The quantities listed are gain normalized voltages sampled at the NCT amplifier outputs and are directly preportioned to the acoustic signals at the NCT locations.

Dynamic data were obtained in two groups during angle of attack sweep from -6° to +6°. Plots of NCT outputs versus angle of attack are presented in Figures 21 through 32.

Interpretation of the digital data is aided by pre-knowledge of the acoustic characteristics of boundary layer signals in a variety of flow conditions. In laminar flow conditions, essentially no wall pressure fluctuations are produced by the boundary layer. Then as Reynolds number is increased in the boundary layer, transition characteristics appear and as Reynolds number continues to increase, full turbulence is observed. In the transition region, boundary layer instabilities occur with "a variety of temporal and spatial patterns" (Swinney & Gollub, Ref. 9) which in our case produce a large mid-frequency amplitude (est. 20-90 khz). As the boundary layer enters into full turbulence (increasingly chaotic) the pressure fluctuation spectrum broadens into higher frequencies and the NCT output is somewhat lower than that in the transition zone.

Table 3

NCT Wind Tunnel Data For

Re_∞ = 4 million/meter

α	NCT Setting	Run No.	N1 (Aft)	N3 (Mid)	N5 (Fwd)	N2 (Aft)	N4 (Mid)	N6 (Fwd)
			(Leeward For Positive)			(Windward for Positive)		
0	Null	1059	175	460	610	565	770	675
0	Right	1062	925	1045	1225	465	1300	2025
0	Left	1065	725	1385	775	1000	1270	1865
1.25	Null	1060	165	570	550	500	690	635
1.25	Right	1063	825	1600	1175	400	1165	1850
1.25	Left	1066	600	2060	695	900	1115	1890
2.50	Null	1061	145	675	800	460	660	621
2.50	Right	1064	775	3550	4500	390	1140	1825
2.50	Left	1067	650	4900	1950	850	1010	1755

N1 through N6 are in millivolts, N1 is wideband, N2 - N6 Narrowband filter 60.70 Khz

Table 4

NCT Wind Tunnel Data For

Re_∞ = 8 million/meter

α	NCT Setting	Run No.	N1 (Aft)	N3 (Mid)	N5 (Fwd)	N2 (Aft)	N4 (Mid)	N6 (Fwd)
			(Leeward For Positive α)			(Windward for Positive α)		
0	Null	1069	200	1210	505	1300	1685	1620
0	Right	1072	1050	1990	750	685	1190	4590
0	Left	1075	875	2415	725	1600	1115	3375
1.25	Null	1070	205	945	475	1175	1445	1420
1.25	Right	1073	810	1095	640	500	820	2970
1.25	Left	1076	625	1365	650	975	635	2835
2.50	Null	1071	210	710	475	620	740	1080
2.50	Right	1074	500	630	500	300	955	2230
2.50	Left	1077	285	875	600	465	715	2160

N1 through N6 are in millivolts, N1 wideband, N2-N6 narrowband filter 60 - 70 Khz

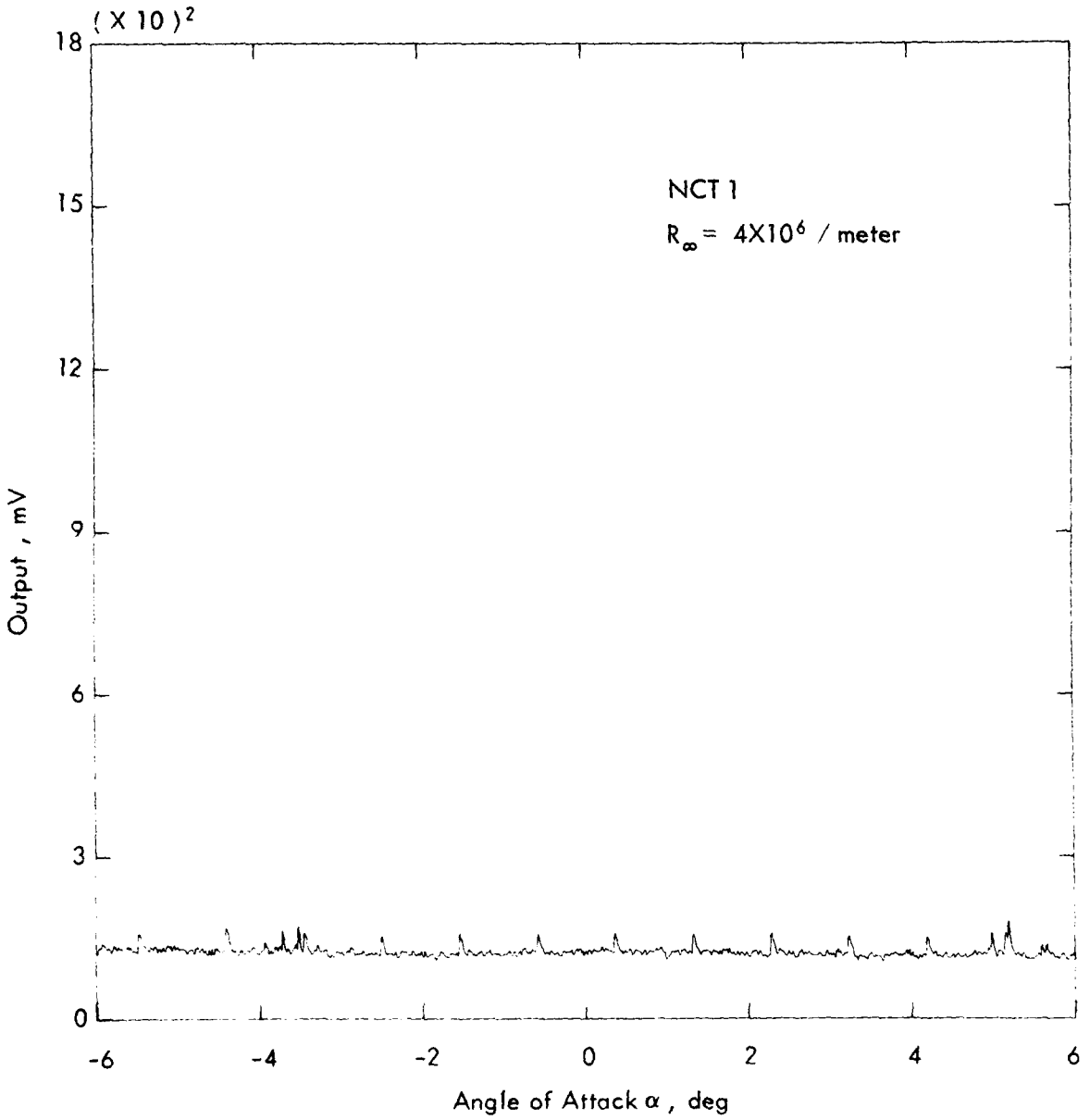

Figure 21. NCT 1 - vs - Alpha (Broadband)

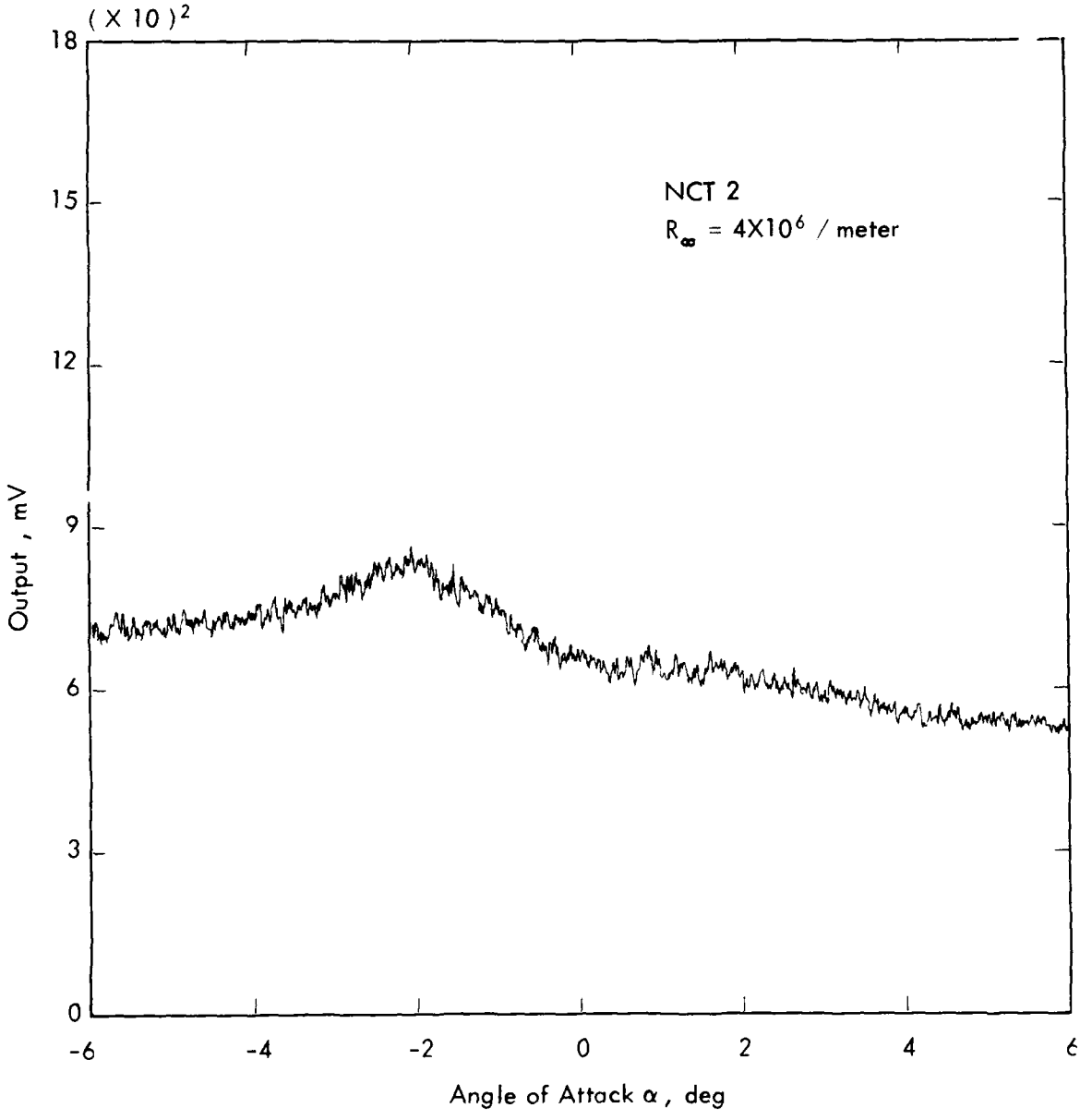

Figure 22 . NCT 2 - vs - Alpha

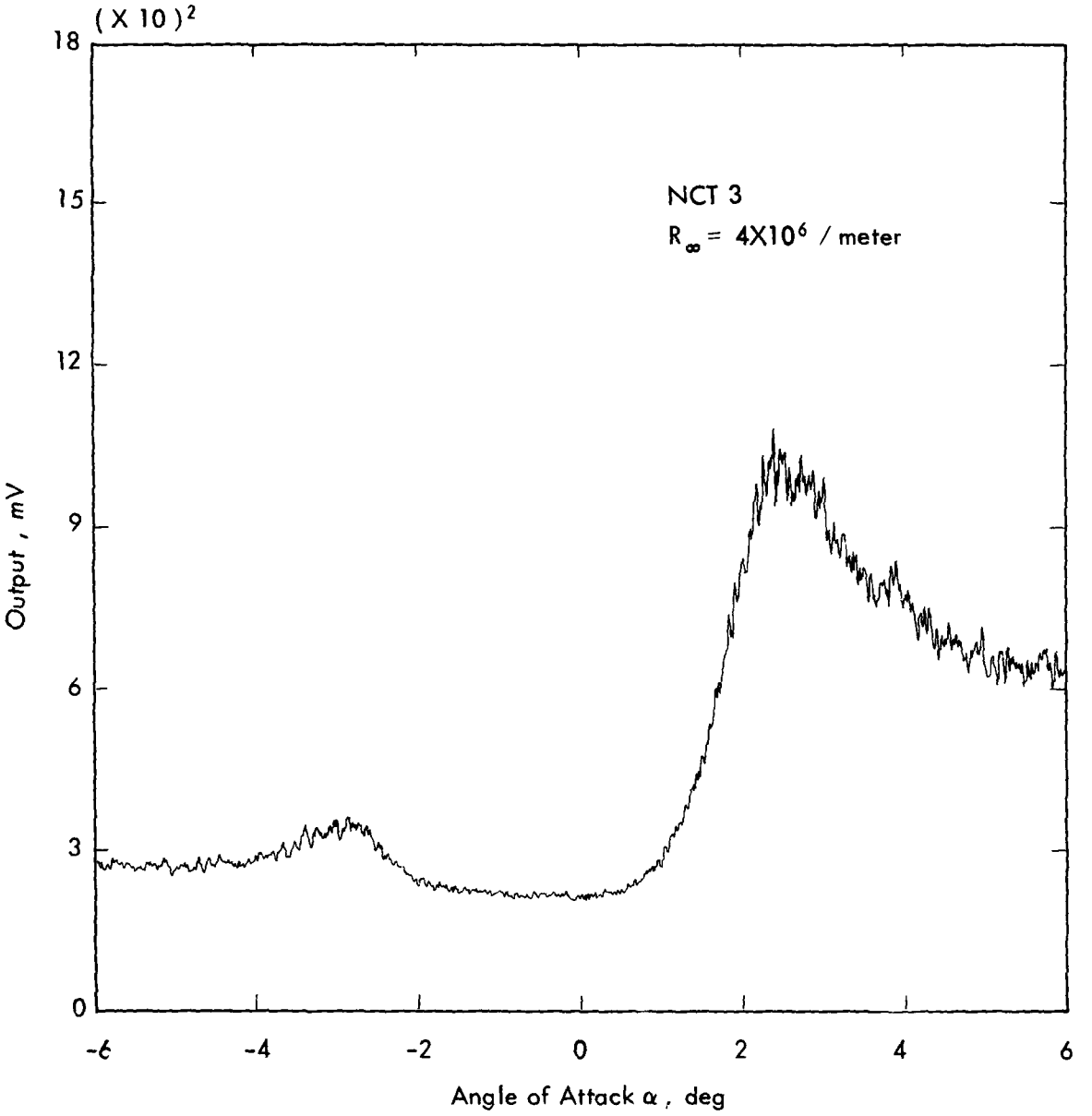

Figure 23. NCT 3 - vs - Alpha

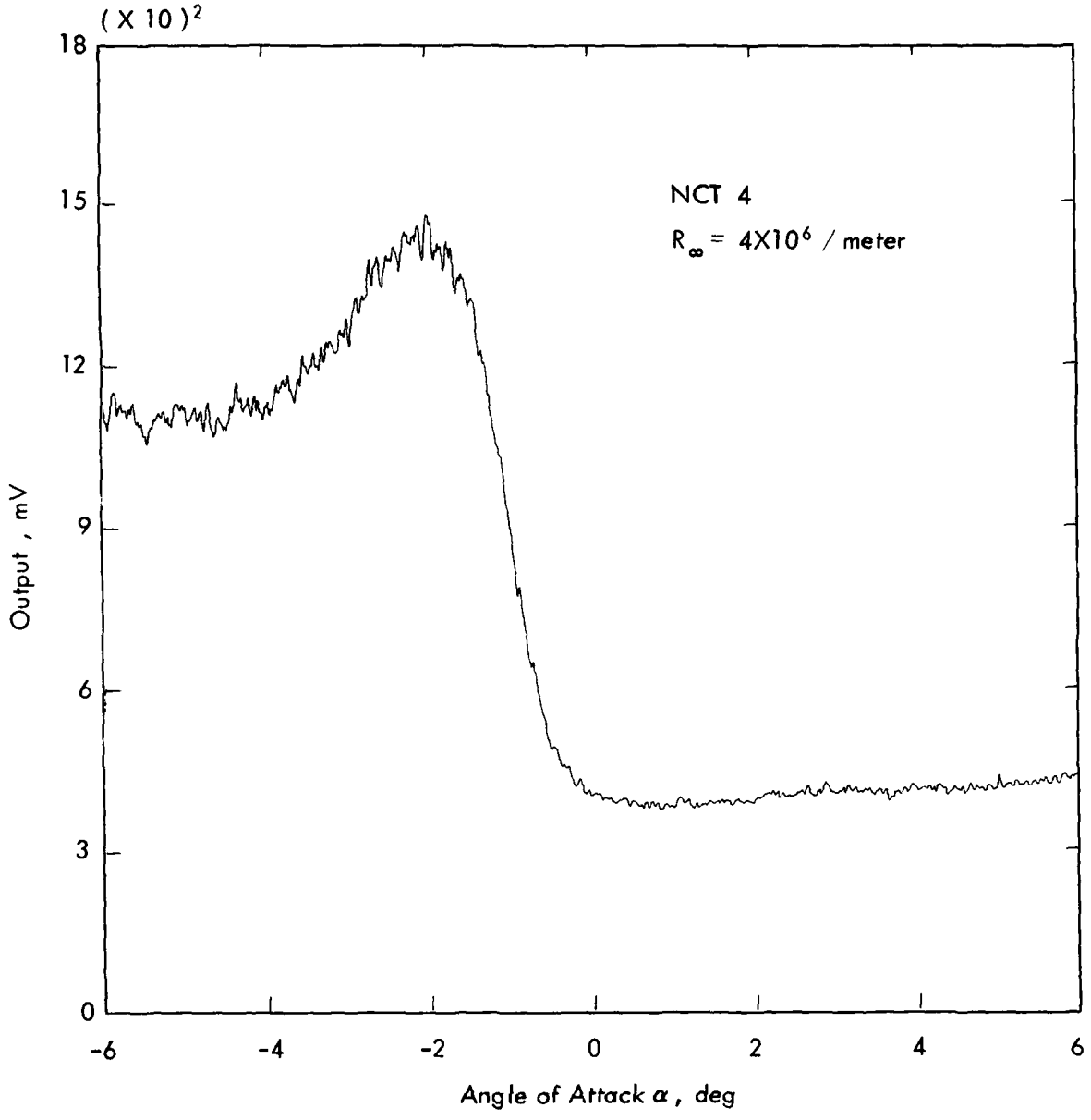

Figure 24. NCT 4 - vs - Alpha

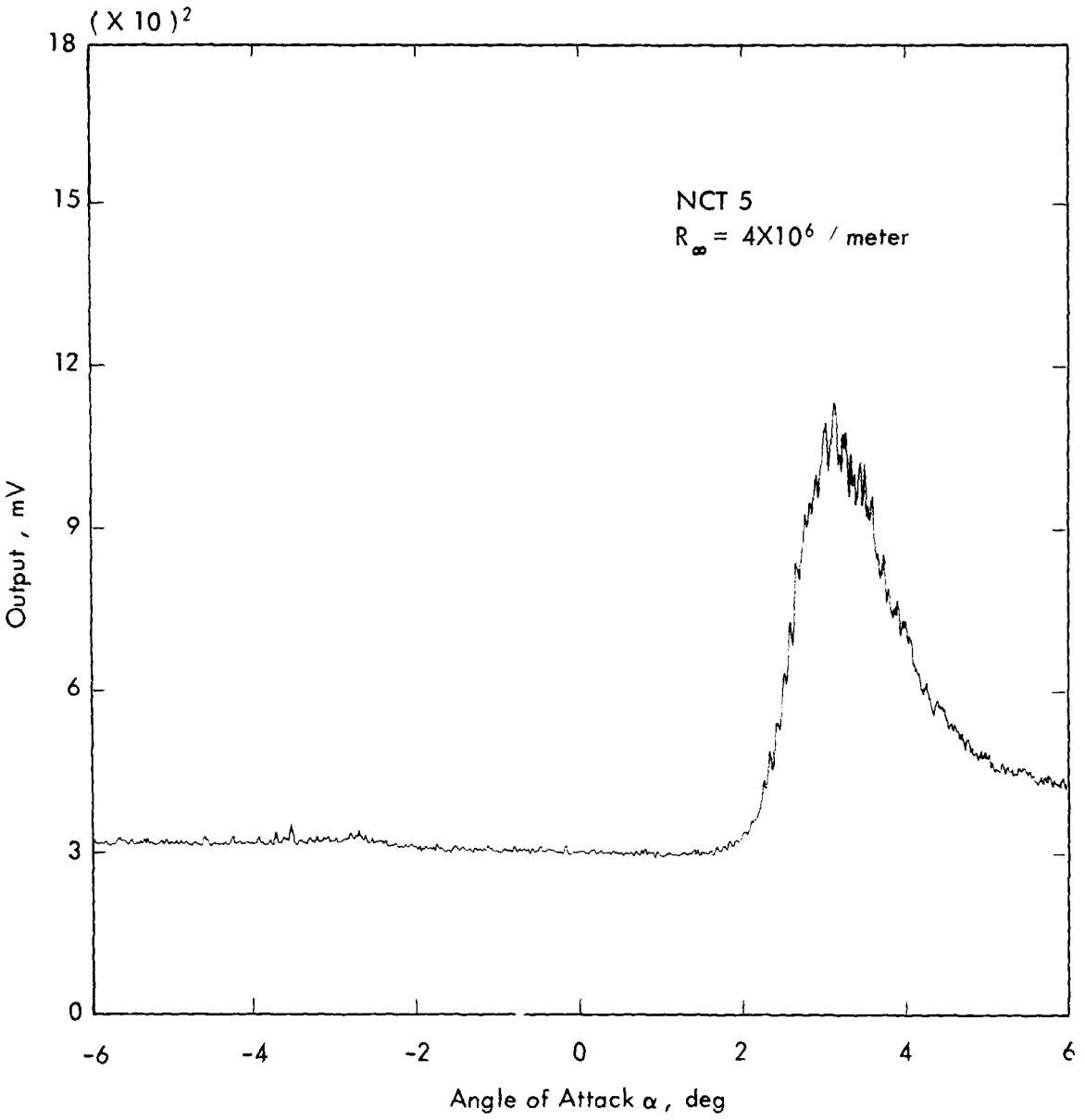

Figure 25. NCT 5 - vs - Alpha

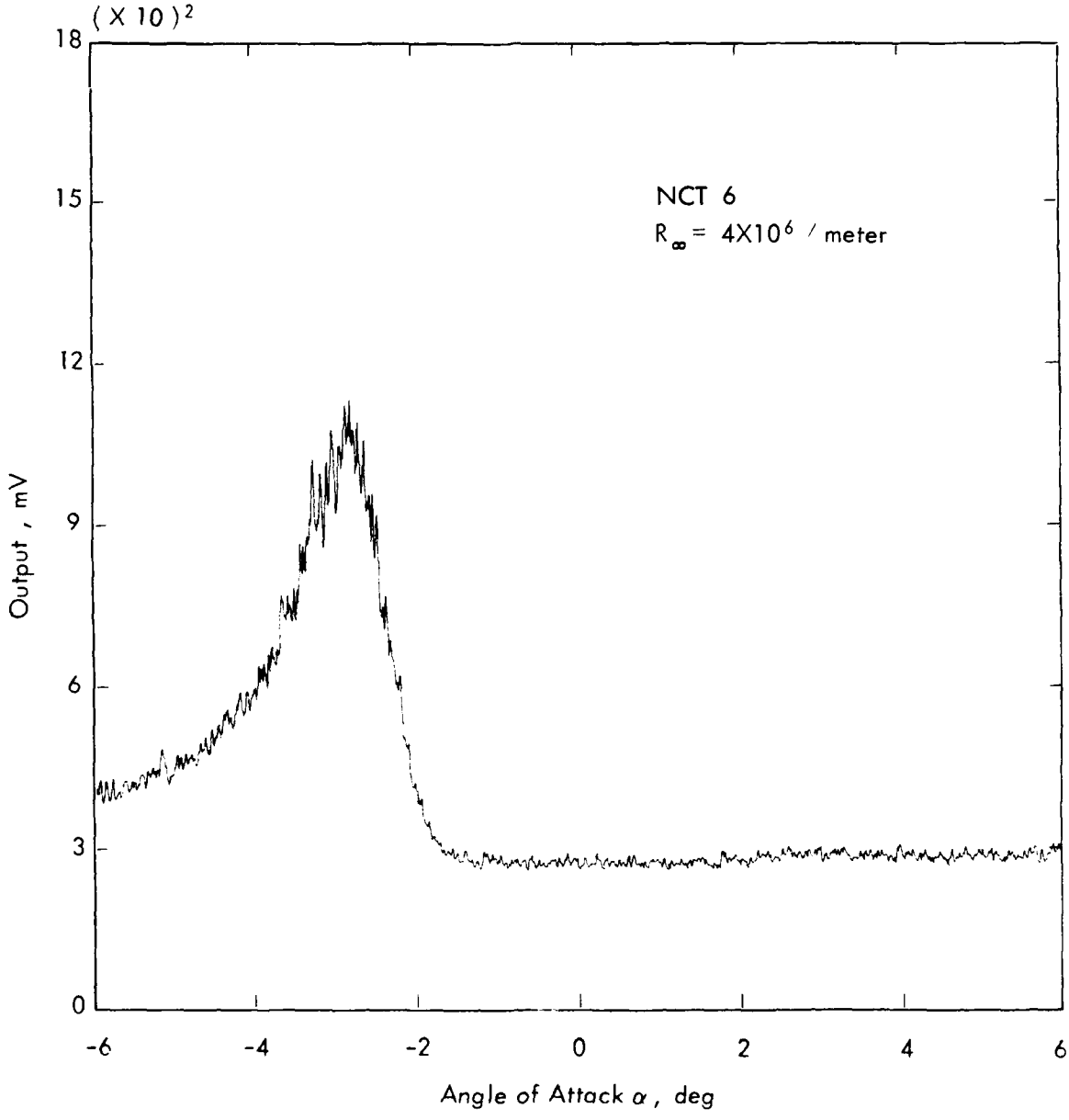

Figure 26 . NCT 6 - vs - Alpha

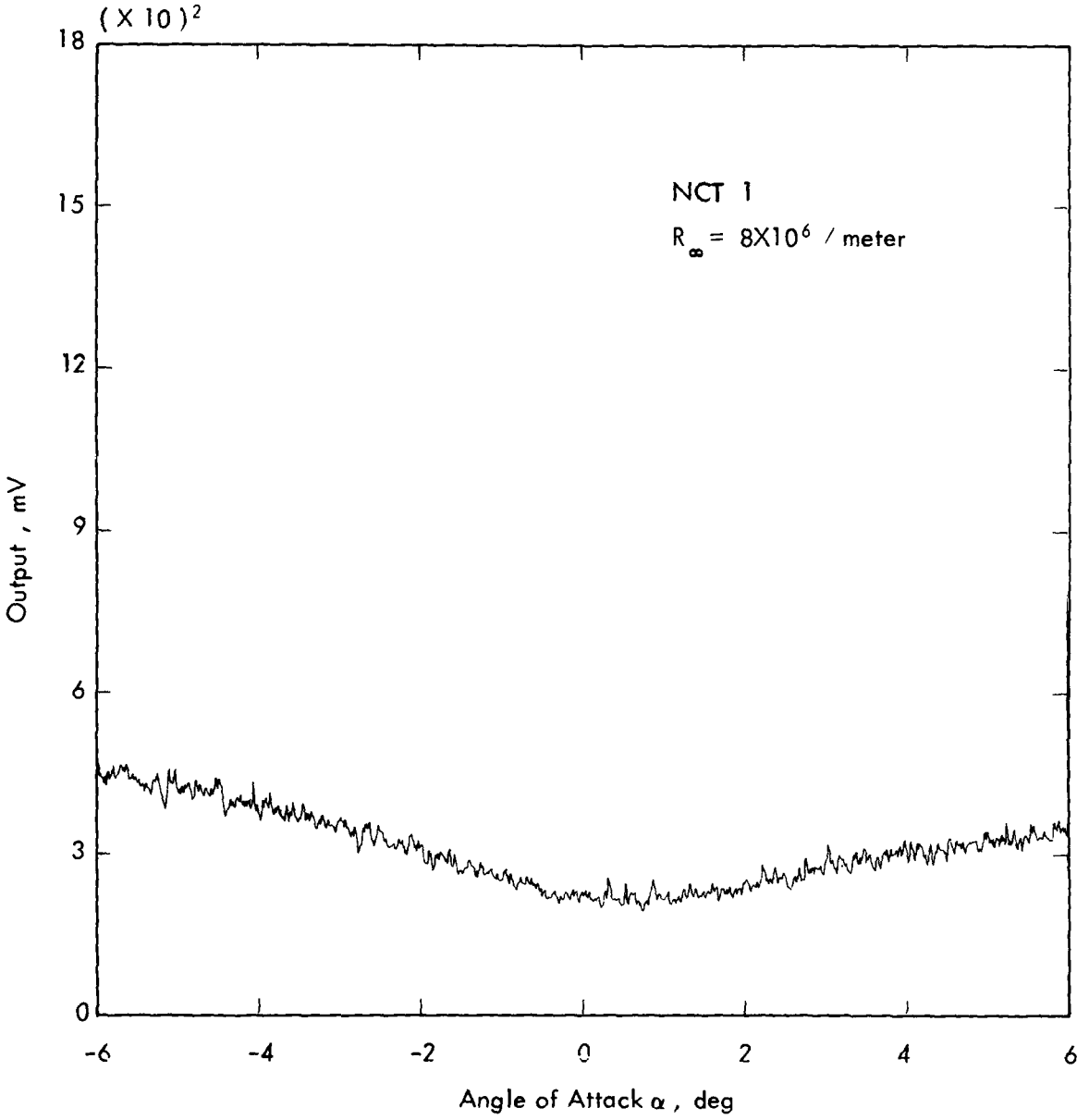

Figure 27. NCT 1 - vs - Alpha (Broadband)

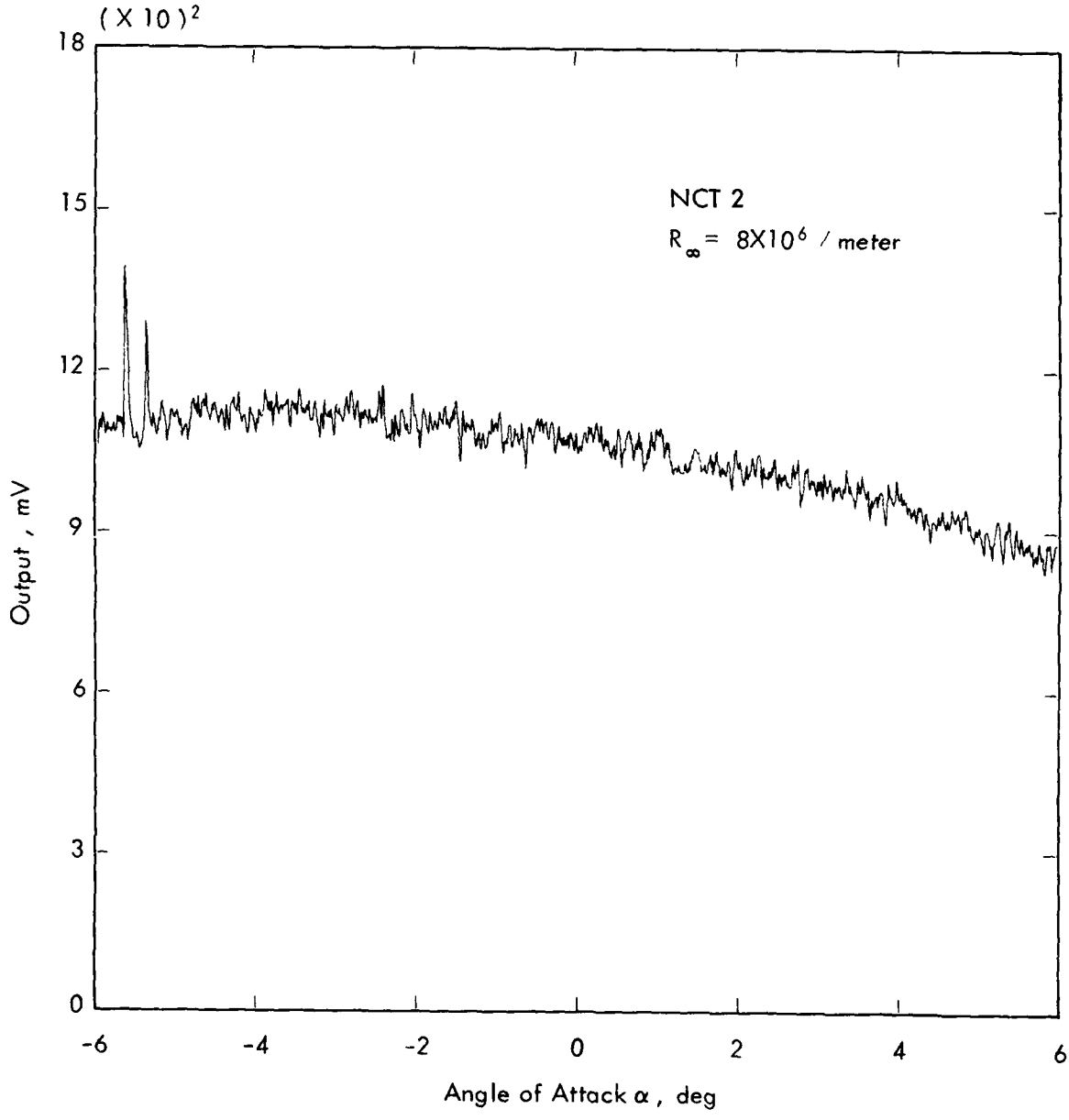

Figure 28. NCT 2 - vs - Alpha

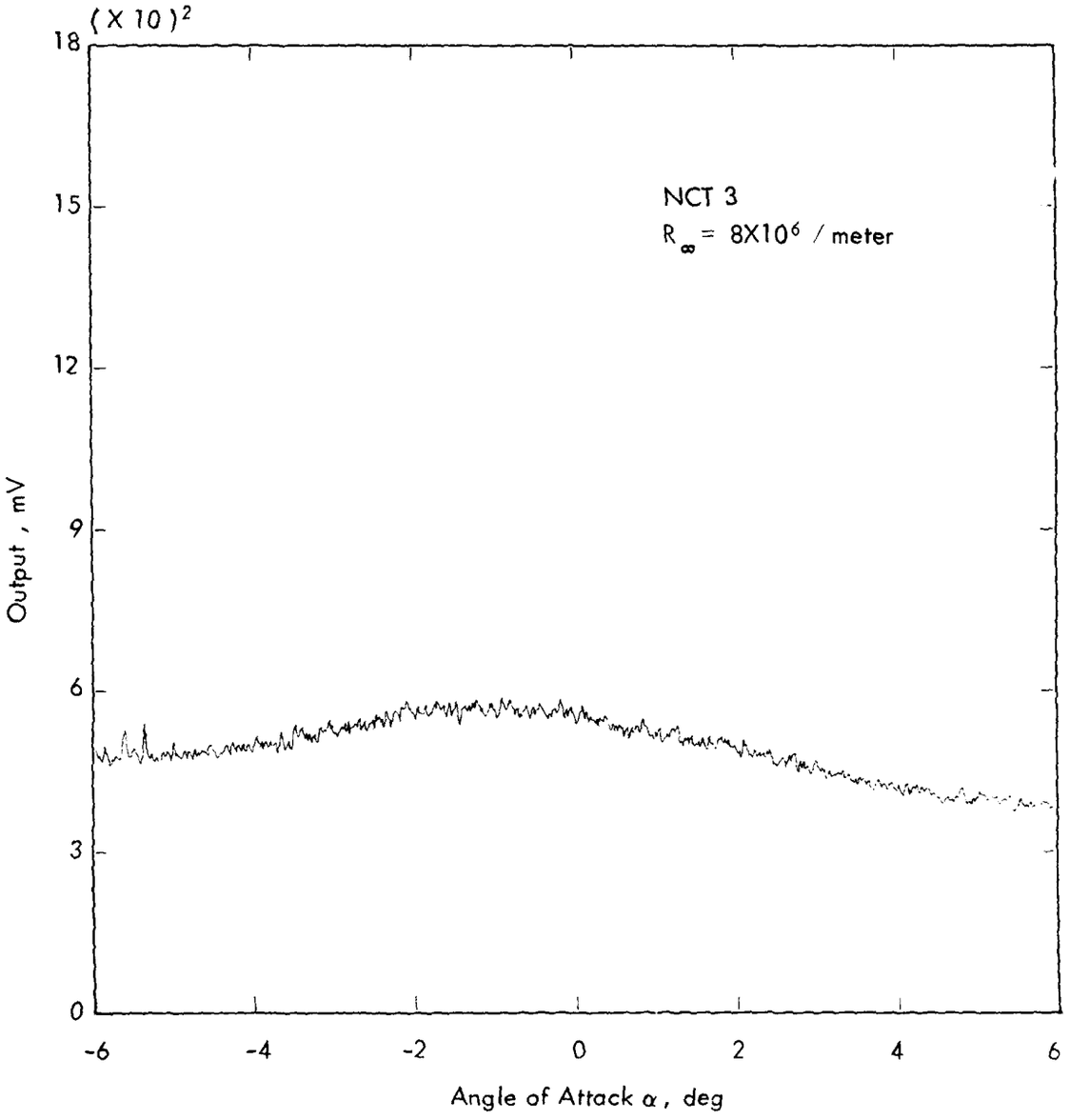

Figure 29. NCT 3 - vs - Alpha

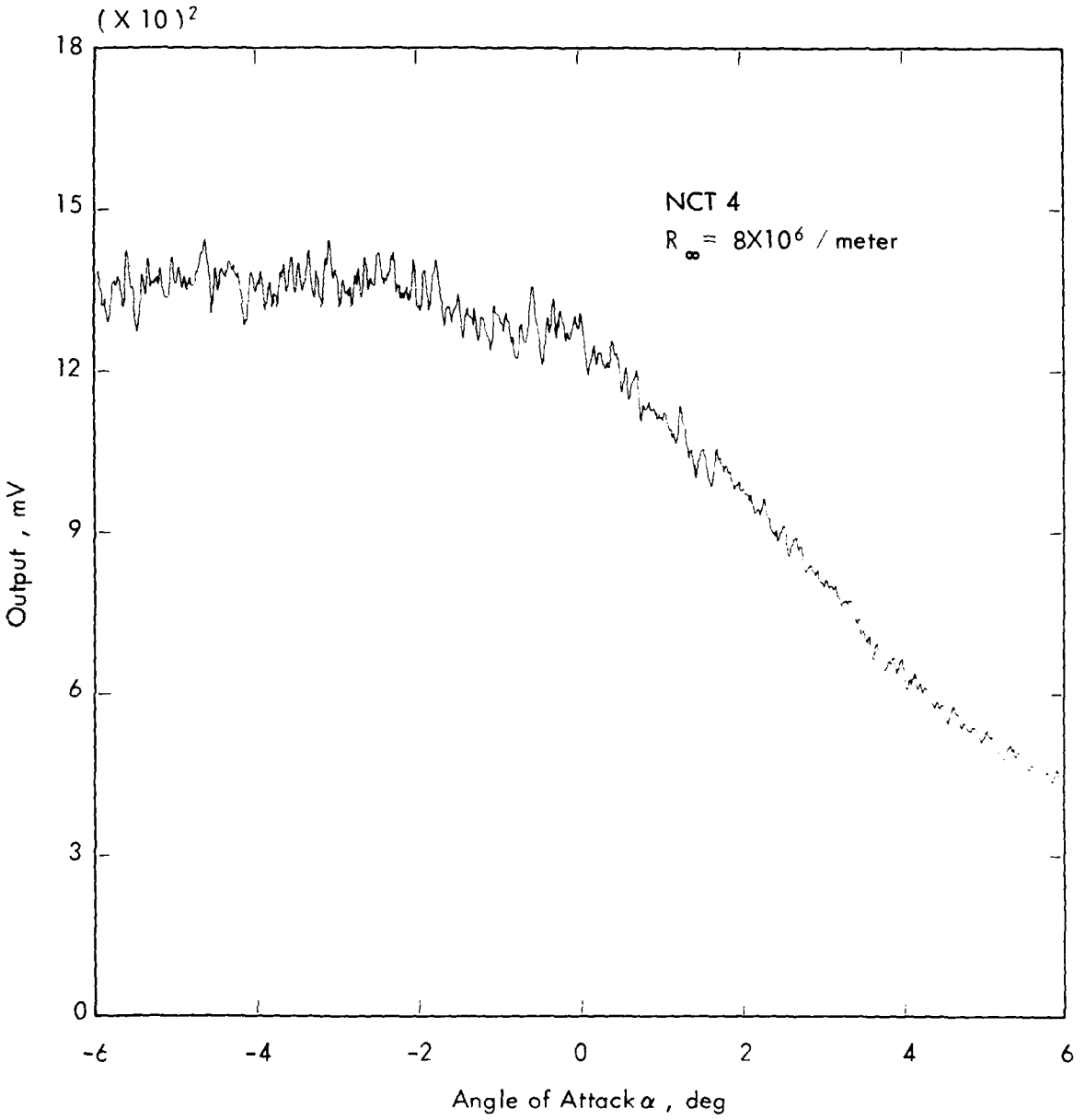

Figure 30. NCT 4 - vs - Alpha

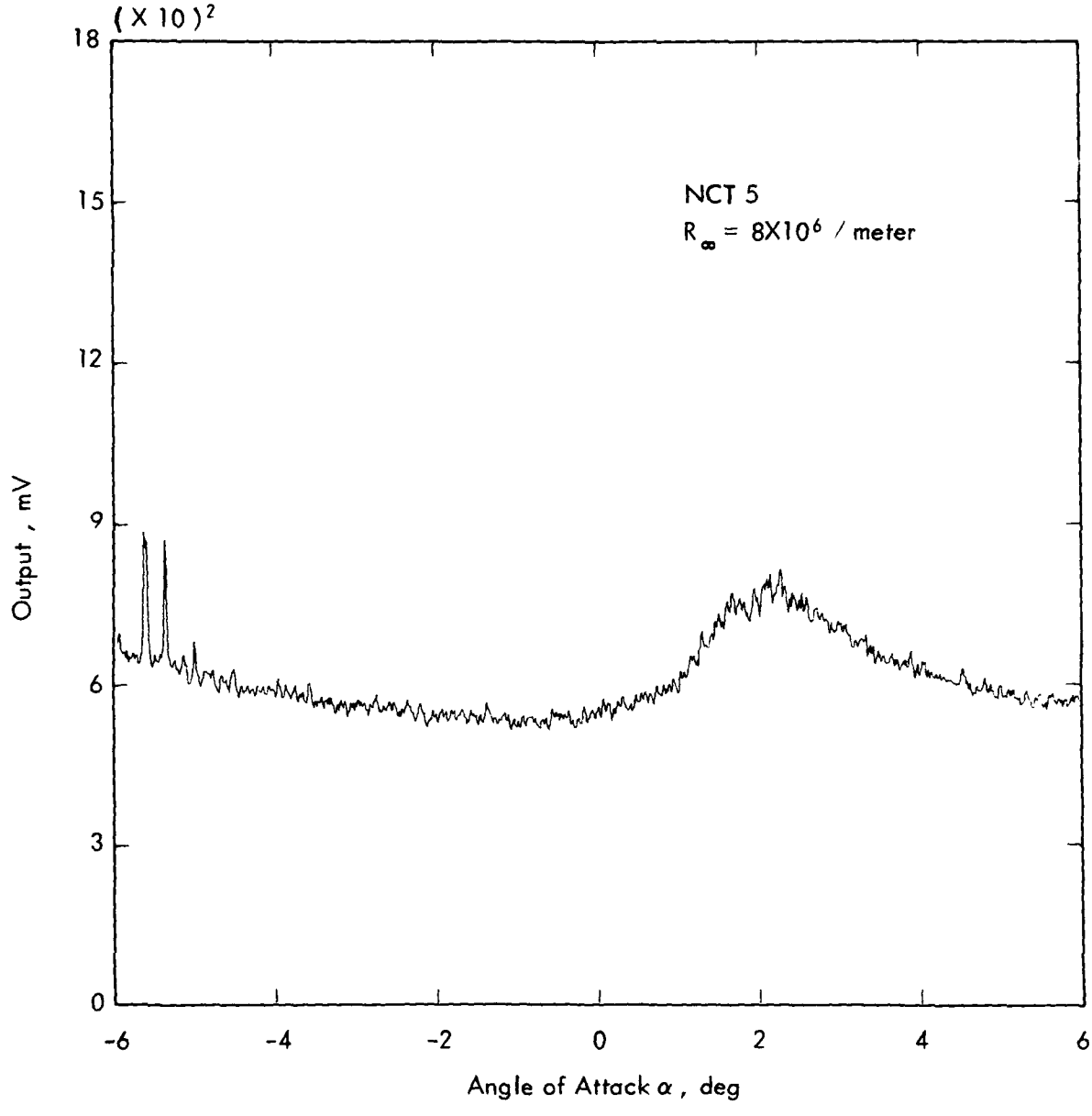

Figure 31. NCT 5 - vs - Alpha

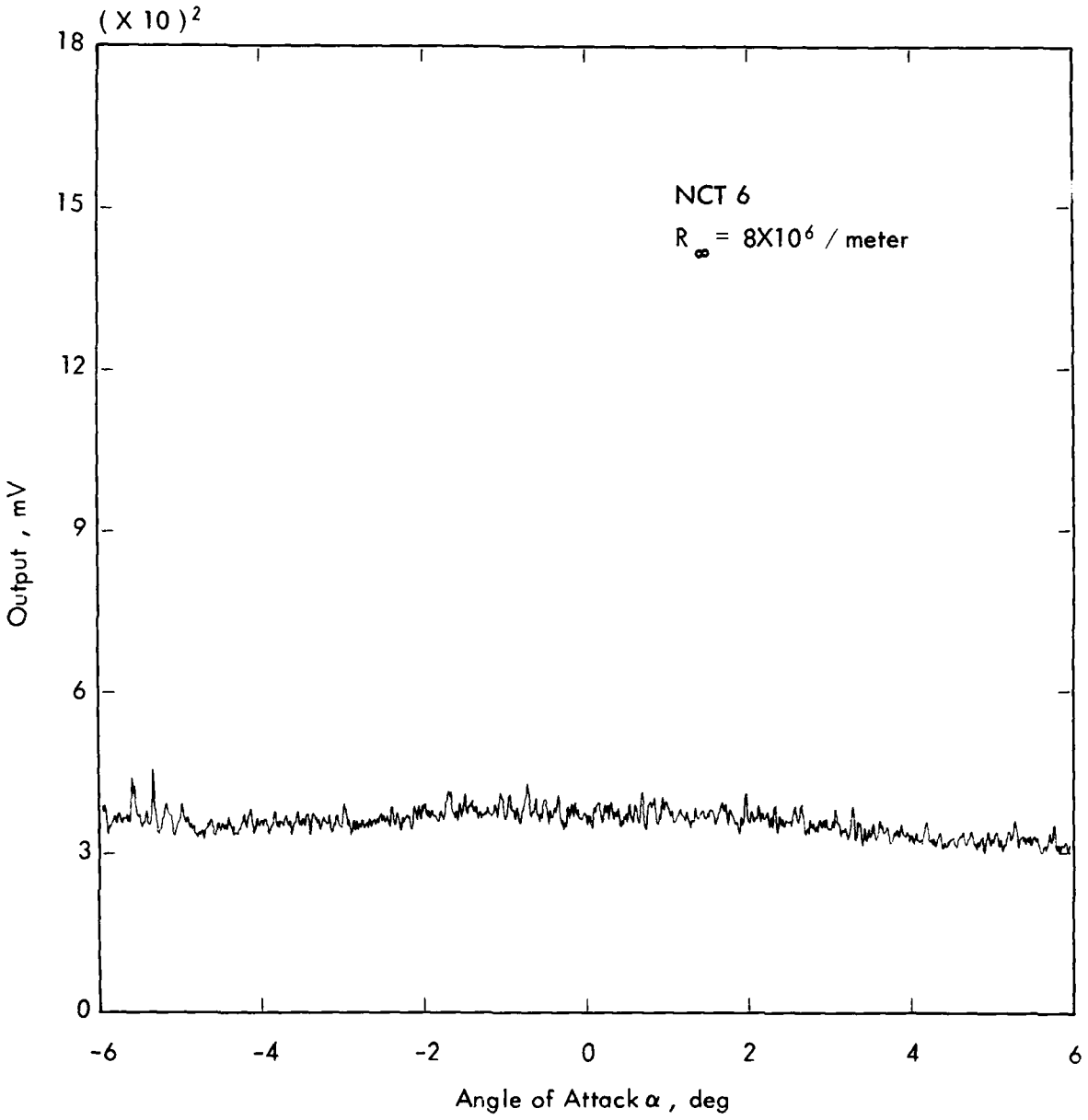

Figure 32. NCT 6 - vs - Alpha

A voltage proportional to the background tunnel noise is always present in the NCT output which can mask the presence of the boundary layer signals. The interpretation of the output is made more difficult with this background noise because of its similarity in many respects to the boundary layer signals. Analysis of some of the data depends on relative amplitude and changes or trends caused by a parameter variable such as Reynolds number which varies a greater percentage than the background noise.

The static data in Table 3 indicate that transition at zero angle of attack is located forward of N1, N2 (station 78 cm) but aft of N3, N4, (Station 61 cm). It may also be observed that as angle of attack is increased transition moves forward on the leeward ray (N1, N3, N5) but the levels remain the same or decrease slightly on the windward ray (N2, N4, N6). Levels shown in Table 3 should be used with caution when comparing one channel to another because absolute calibration of the transducers was not possible. Also note that the level of N1 data has been influenced by the amplifier bandwidth and is lower because the Channel 1 gain was low.

The narrowband data of channels N2 through N6 provided better transition measurement than did the broadband data of channel N1, an observation best illustrated by the NCT null output dynamic data in Figure 21 and Figure 22. If channels 1 and 2 data were conditioned identically the results would have been symmetrical change in signal level with respect to α as was observed for channels 3 and 4 (Figures 23 and 24) and channels 5 and 6 (Figures 25, 26).

Figures 23 through 26 illustrate the capability of the NCT to measure transition in that excellent signal-to-noise data were obtained and the relative levels during the sweep were as expected. Features of these traces were the sharp

rise of the signal to a maximum level followed by a reduction to a level higher than laminar but lower than the transition peak. The final level is indicative of full turbulence at the transducer location.

The static and dynamic data for Reynolds number of 8 million/meter indicate that transition on the model is forward of the N5, N6 (station 46 cm). The dynamic data shown in Figures 28-32 for Re_∞ of 8 million/meter show a laminar-transition-turbulence trend but with little contrast as was seen in Figures 23-26 for the lower Reynolds number of 4 million/meter.

It had been expected that the NCT noise improvement concept would have been verified by the wind tunnel test static data. Using Table 3 and comparing levels of right, left and null NCT settings, the data indicate that the null setting reduced the signal-to-noise level rather than increasing it. Fairly large ratios of levels from right and left to null settings were obtained but where transition was occurring (e.g. N3 and N5 at α = 2.5°) the null setting apparently reduced the boundary layer signal more than the noise. The reason for this unexpected result may be that the crystals of the NCT sensor were placed too close with the result that the boundary layer signals at the two crystals were highly correlated and were reduced significantly in the subtraction process.

3.2.3 Broadband Analog Data

Analog broadband magnetic tape recordings were made of the data from five of the six NCT channels. The sixth (channel 1) was not recorded due to amplifier failure at test time. The recording bandwidth was 500 khz but the overall system was

limited to approximately 100 khz due to the sensor preamplifier output impedance and the 40 feet of cable from the model to the signal conditioning chassis.

Selected NCT broadband signal records have been examined to determine if correlation exists to the digital data presented in the preceding section. These records, for channels 3 and 5 are shown in Figures 33 through 38 are plots of spectrum analyzer traces obtained by tape playback through a spectrum analyzer then to an x-y plotter. Flow and mode conditions for the data are given in the figures; the Reynolds number was constant at 4 million per meter. The data group number has been placed on each of the figures so that comparison may be made with the data in Table 3 in which the narrowband d.c. output data are listed for these same data groups.

The quality of the broadband signals shown in Figures 33-38 is not very good because the signal-to-noise ratio is low. The two principal contributors to the low S/N ratio were the boundary layer signal and a poor choice of the point to pick off the NCT signal. (Broadband data was taken directly from the center terminal of the balance potentiometer; a better choice would have been to take the signal out after one or two stages of amplifications).

Boundary layer signals can be seen in Figures 34 and 35 for channel 3 and in Figures 37 and 38 for channel 5; locations of the signals are marked on each of these figures. The appearance of relatively large signals in this group correlates well with the large amplitudes noted for the same groups in Table 3. The increase occurs in channel 3 data at a lower angle of attack (1.25°) than in channel 5 which is expected because channel 3 is further aft than channel 5.

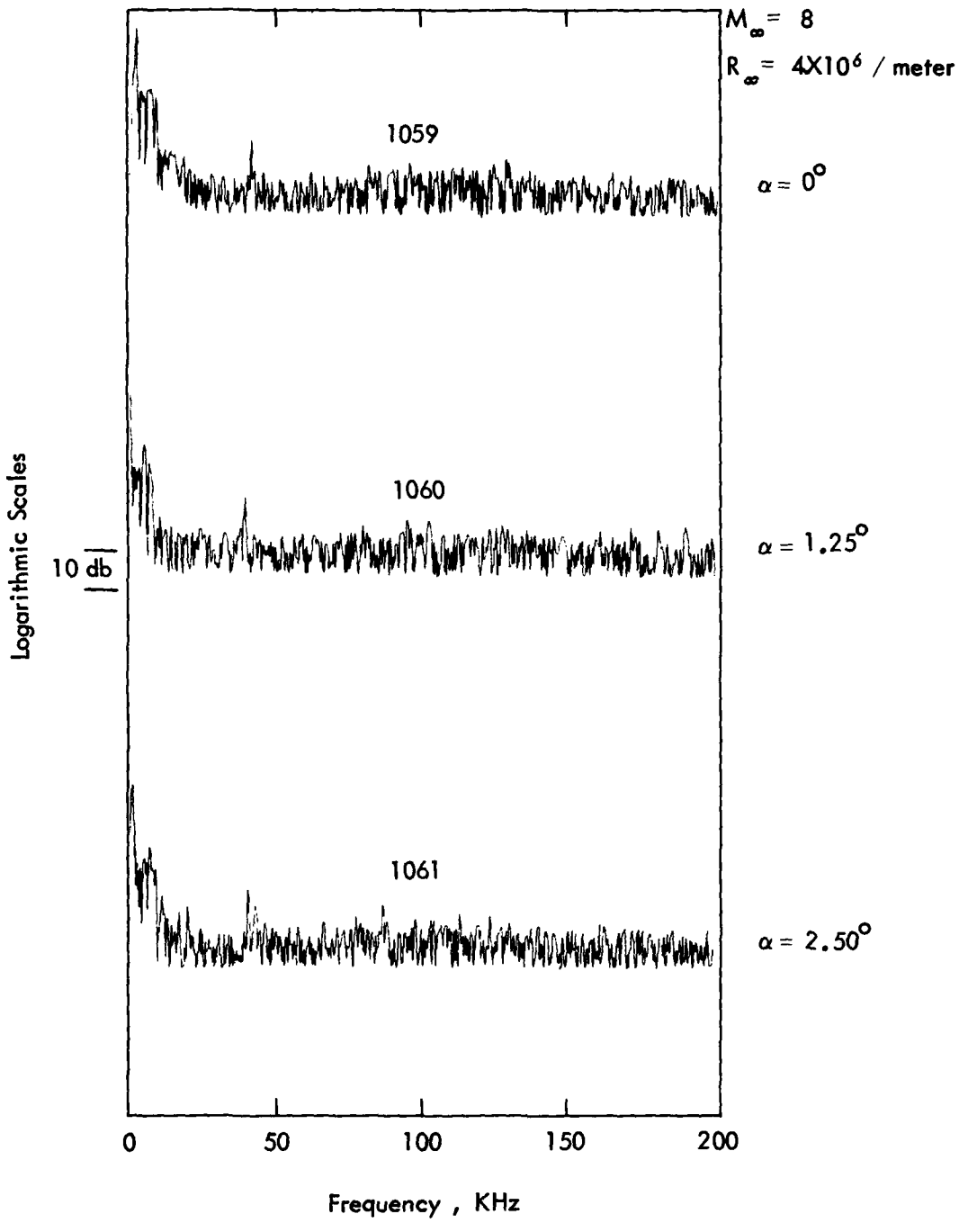

Figure 33. NCT 3 Spectrum , Null Setting

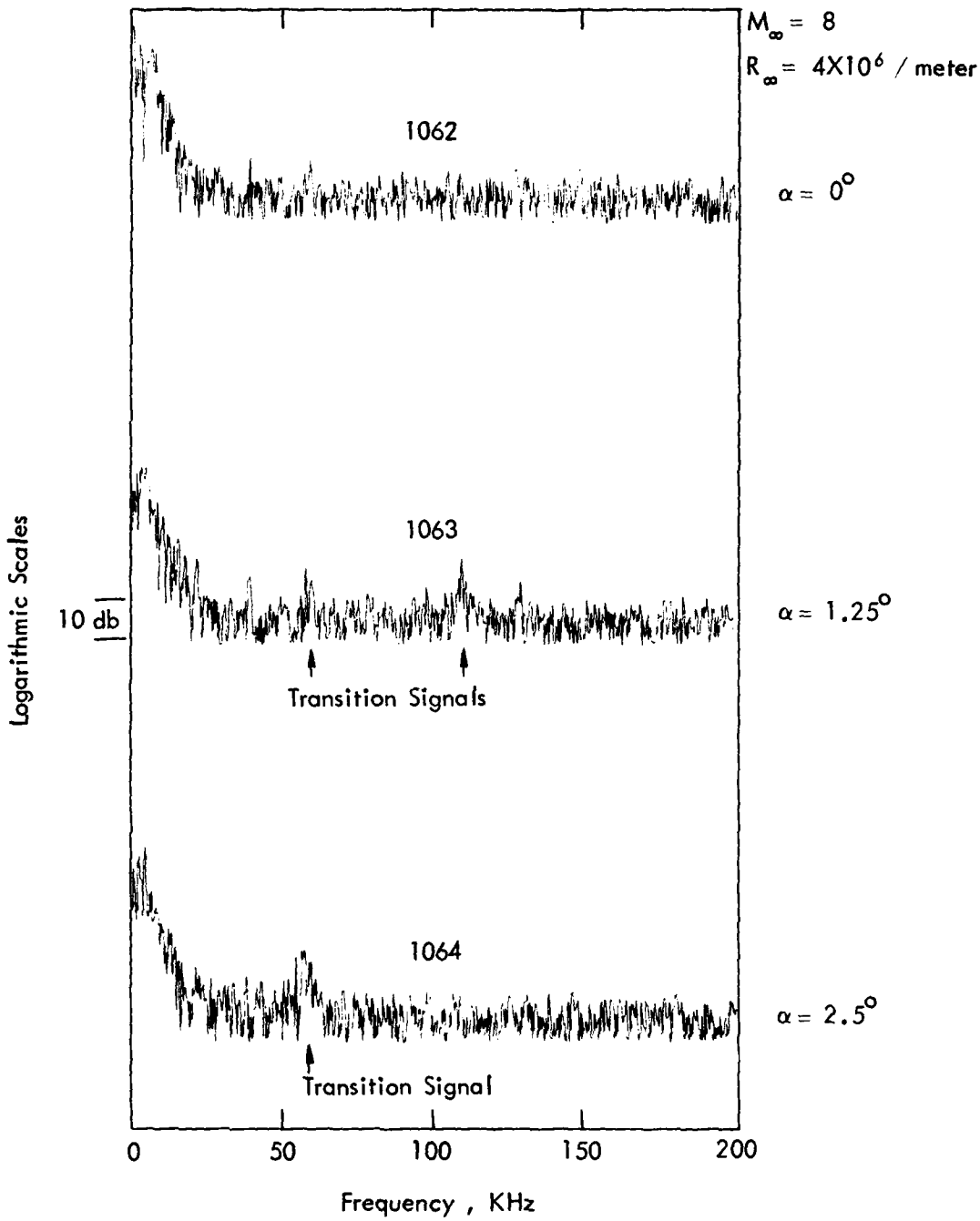

Figure 34. NCT 3 Spectrum, Right Setting

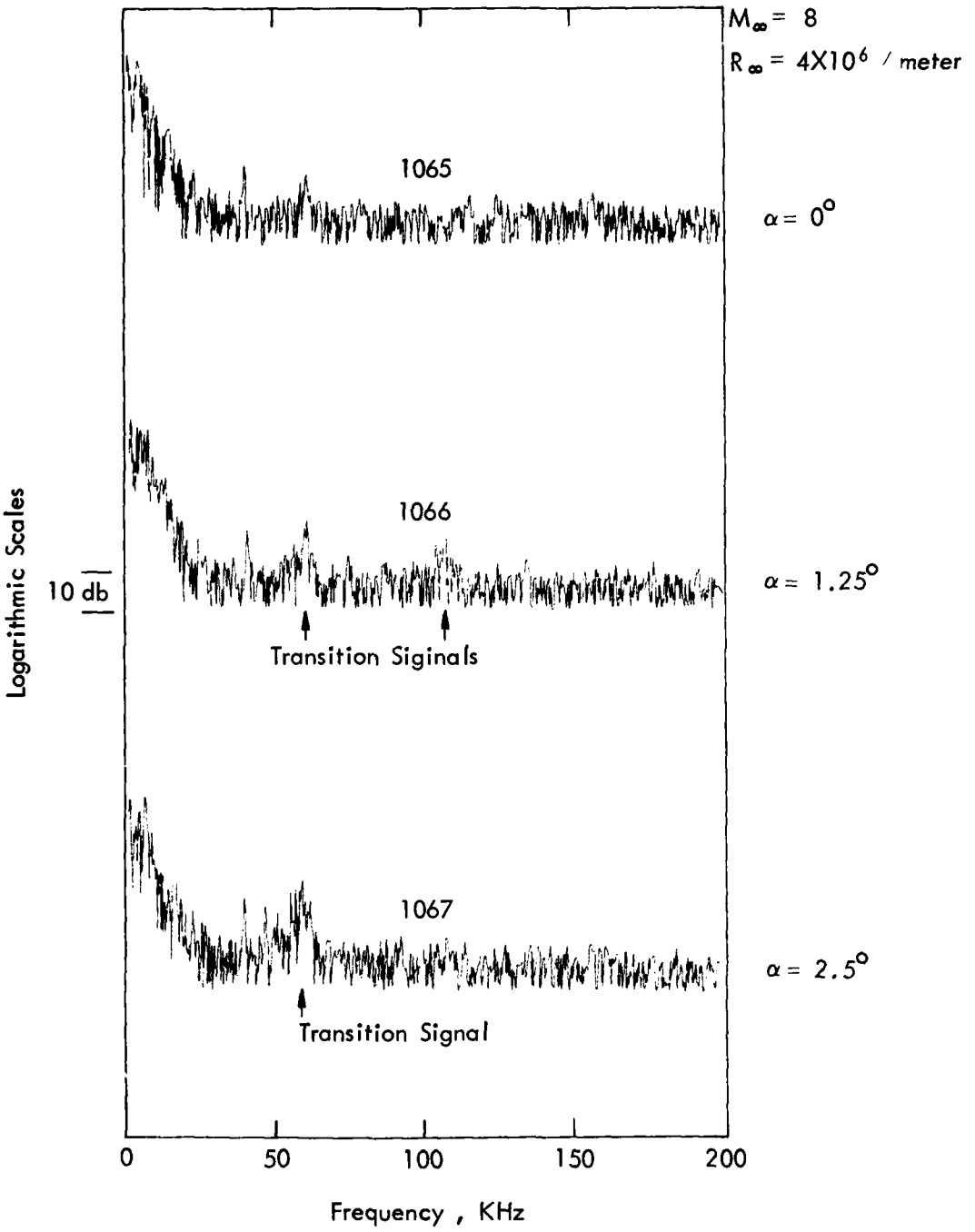

Figure 35. NCT 3 Spectrum , Left Setting

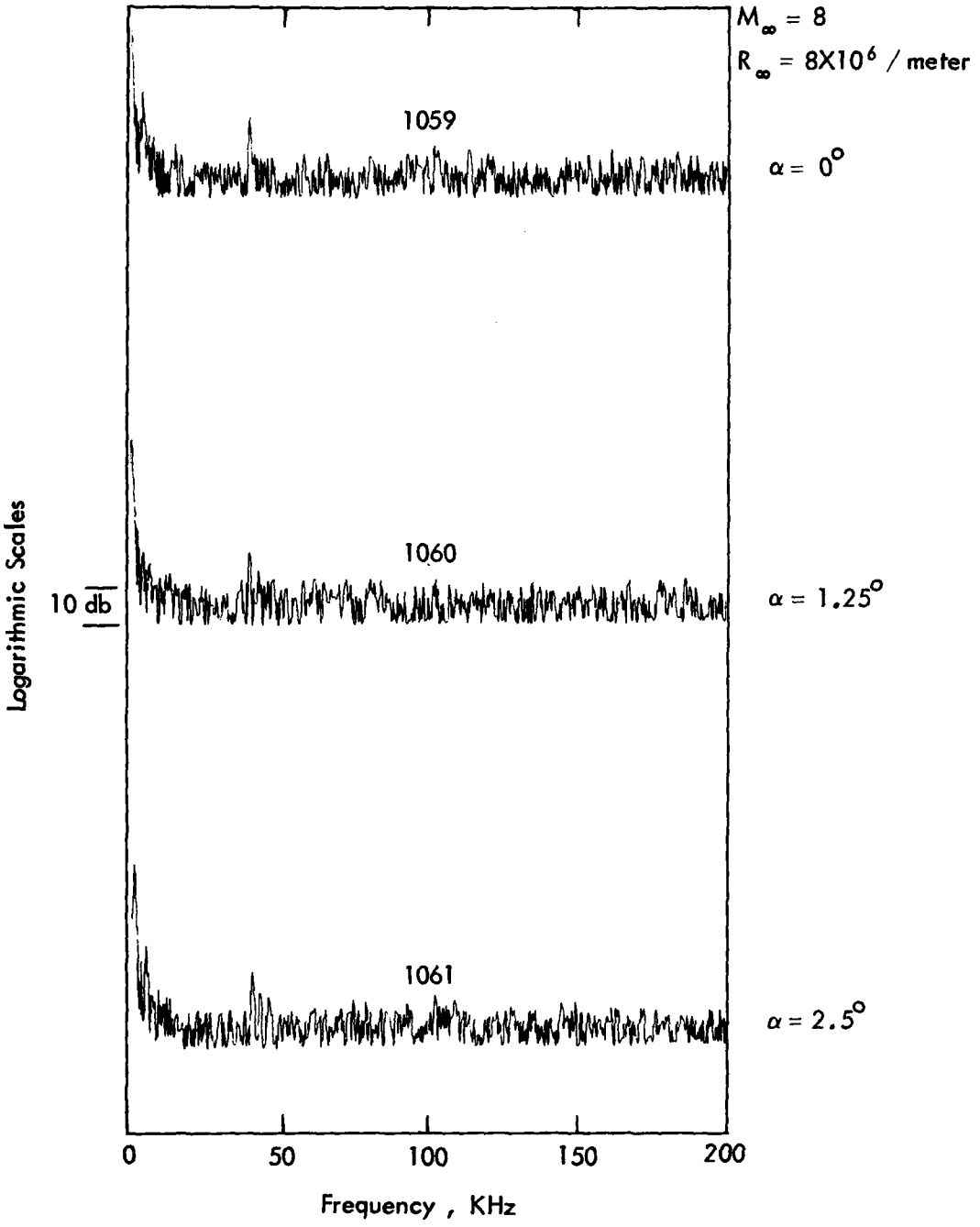

Figure 36 . NCT 5 Spectrum , Null Setting

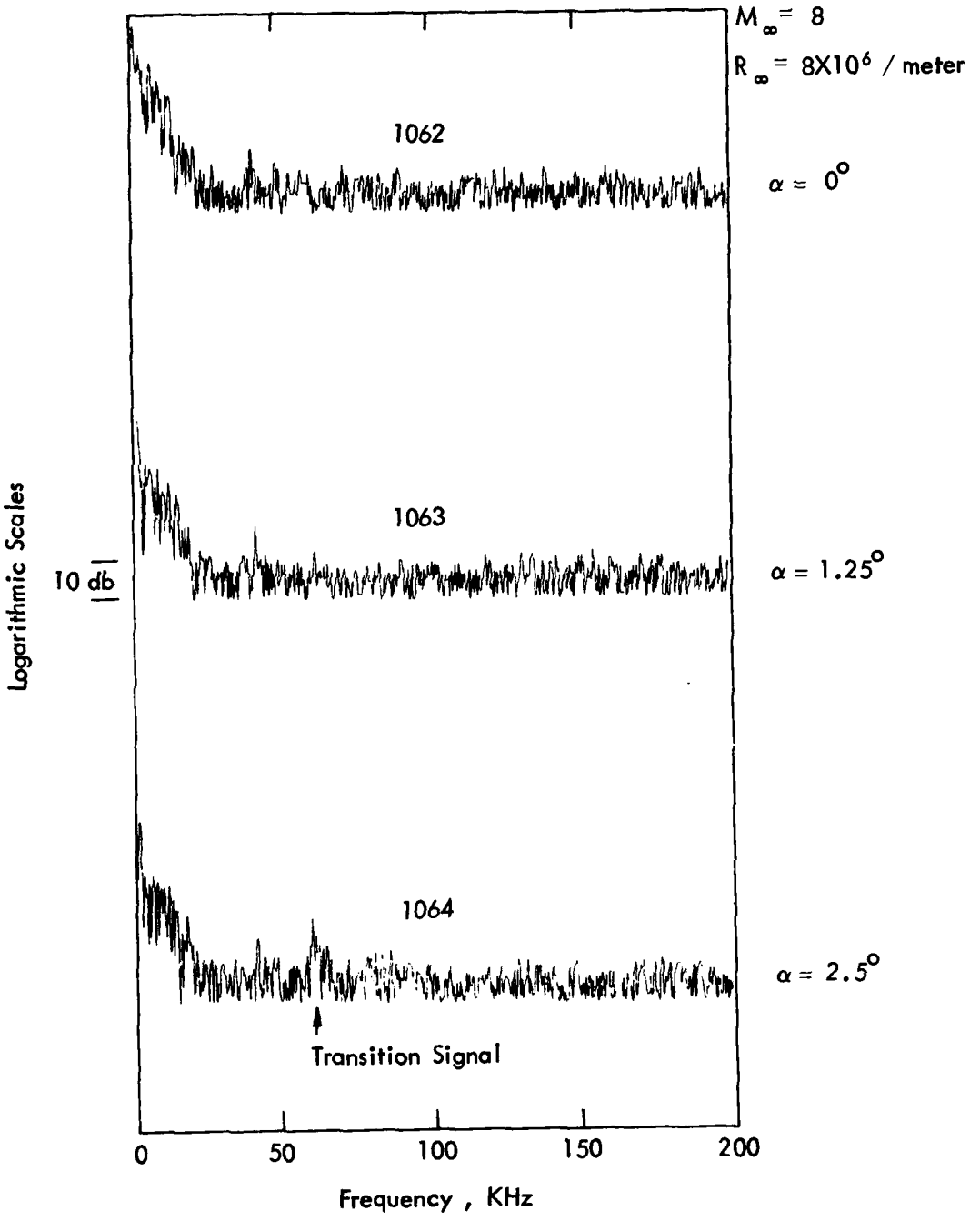

Figure 37. NCT 5 Spectrum , Right Setting

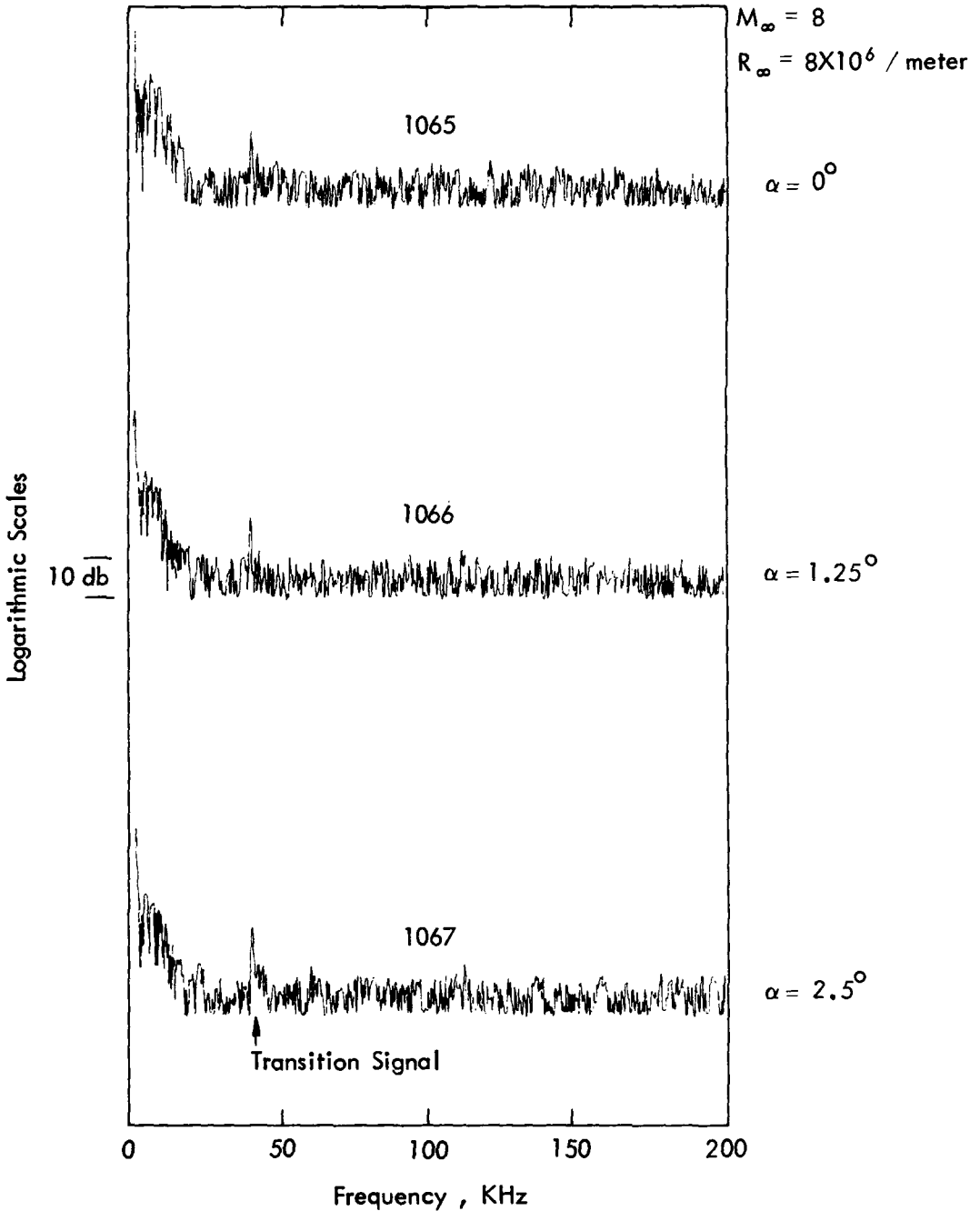

Figure 38. NCT 5 Spectrum , Left Setting

It should be noted that boundary layer spectra containing broad peaks have been observed by another experimenter using a hot wire anemometer in the transition of pre-transition zone of the boundary layer flow.[12] The broad peaks of the transition spectrum give away to a more continuous monotonic spectrum as the flow becomes fully turbulent. The exact mechanism which creates this type of transition spectrum is not fully known nor is its relationship to the traditional boundary layer parameters known complete enough to predict the characteristics of the spectrum.

The broadband data also seem to affirm that the cancellation feature of the NCT was not operating as theorized. The evidence for this conclusion is that the data in Figures 33 and 36 taken with the NCT set in the null positions show no or minimal boundary layer signal. Cancellation is present as evidenced by the lower levels around the zero frequency marker on the plots for null setting compared to either the left or right settings.

This indicates that the boundary layer signal was probably highly correlated between the right and left sensors and was cancelled in the subtraction process.

4.0 CONCLUSIONS AND RECOMMENDATIONS

A noise cancellation transducer was developed and tested on this program. The results presented in Section 3.0 showed that boundary layer signals can be measured with good signal-to-noise ratio in high noise background wind tunnel tests.

The NCT function was partially validated in the small model test wherein it was noted that the cross-flow transducer produced a significantly higher transition signal than did the parallel flow transducer. It is believed that the transducer crystals were too close together to permit good cancellation data in the AEDC Test where the boundary layer was thicker.

Recommendations for further work include the following:

1) Additional testing with an NCT with larger crystal spacing.

2) Determination of the optimum frequency band with which to distinguish the boundary layer conditions.

3) Testing in comparison with older established methods to permit better understanding and acceptance of the acoustical signal method.

REFERENCES

1. R. T. Winnicki, V. Peckham, "Acoustic Transition Monitor Program Report Volume I Blam Characterization and Development," Kaman Sciences Corp. Report No. K-79-16R, January 1979.

2. W. W. Willmarth, "Space-Time Correlation of the Fluctuating Wall Pressure in a Turbulent Boundary Layer," Journal of the Aeronautical Sciences, Vol. 25, No. 5, May 1958.

3. A. L. Kistler and W. S. Chen, "The Fluctuating Pressure Field in a Supersonic Turbulent Boundary Layer," Journal of Fluid Mechanics, Vol. 16, pt. 1, May 1963.

4. C. F. Coe, "Surface Pressure Fluctuations Associated with Aerodynamic Noise," Basic Aerodynamic Noise Research, 1970.

5. J. S. Serafini, "Wall-Pressure Fluctuation and Pressure-Velocity Correlations in a Turbulent Boundary Layer," NASA TR R-165, Dec. 1963.

6. W. V. Speaker and C. M. Ailman, "Spectra and Space-Time Correlations of the Fluctuating Pressures at a Wall Beneath a Supersonic Turbulent Boundary Layer Perturbed by Steps and Shock Waves," NASA CR-486, May 1966.

7. K. R. Raman, "A Study of Surface Pressure Fluctuations in Hypersonic Turbulent Boundary Layers," NASA CR-2386.

8. J. Dunn, "Recent Wind Tunnel Tests in the Boundary Layer Regime," PDA, Presentation at Accuracy Review Meeting, June 1978.

9. H. L. Swinney and J. P. Gollub, "The Transition to Turbulence," Physics Today, August 1978.

10. V. Peckham, Vol. I "Bounary Layer Measurement Program-Boundary Layer Acoustic Monitor Development Characteristics and Installation," Kaman Sciences Corp., Report No. K-79-3U, January 1979.

11. A. Demetriades, "Wind Tunnel Evaluation of a Submerged Boundary Layer Transition Sensor at Supersonic Speeds," Ford Aeronautic and Communications Corp., Report No. U-6459, Sept. 1978.

12. A. Demetriades, "Hydrodynamic Stability and Transition to Turbulence in the Hypersonic Boundary Layer over a Sharp Cone," Ford Aeronautic and Communications Corp., Report No. U-6139, April 15, 1975.

DISTRIBUTION LIST

DEPARTMENT OF DEFENSE

Assistant Secretary of Defense
Atomic Energy
ATTN: Executive Assistant

Defense Advanced Rsch. Proj. Agency
ATTN: TIO

Defense Intelligence Agency
ATTN: DT-2
ATTN: DT-1B

Defense Nuclear Agency
ATTN: STSP
ATTN: SPAS
ATTN: DDST
4 cy ATTN: TITL

Defense Technical Information Center
12 cy ATTN: DD

Field Command
Defense Nuclear Agency
ATTN: FCPR

Field Command
Defense Nuclear Agency
Livermore Division
ATTN: FCPRL

Joint Chiefs of Staff
ATTN: J-5 Nuclear Division

Joint Strat. Tgt. Planning Staff
ATTN: JLTW-2
ATTN: JPTM

NATO SCHOOL (SHAPE)
ATTN: U.S. Documents Officer

Undersecretary of Def. for Rsch. & Engrg.
ATTN: Strategic & Space Systems (OS)

DEPARTMENT OF THE ARMY

BMD Advanced Technology Center
Department of the Army
ATTN: ATC-M

BMD Program Office
Department of the Army
ATTN: Technology Division

Deputy Chief of Staff for Ops. & Plans
Department of the Army
ATTN: DAMO-NCZ

Deputy Chief of Staff for Rsch., Dev., & Acq.
Department of the Army
ATTN: DAMA-CSS-N

Harry Diamond Laboratories
Department of the Army
ATTN: DELHD-N-RBH
ATTN: DELHD-RC

DEPARTMENT OF THE ARMY (Continued)

U.S. Army Ballistic Research Labs.
ATTN: DRDAR-BL, R. Eichelberger

U.S. Army Material & Mechanics Rsch. Ctr.
ATTN: DRXMR-HH

U.S. Army Materiel Dev. & Readiness Cmd.
ATTN: DRODE-D

U.S. Army Missile R&D Command
ATTN: DRDMI-XS

DEPARTMENT OF THE NAVY

Naval Research Laboratory
ATTN: Code 2627 (Tech. Lib.)

Naval Sea Systems Command
ATTN: SEA-0351

Naval Surface Weapons Center
ATTN: Code K06
2 cy ATTN: Code K82

Office of the Chief of Naval Operations
ATTN: OP 604C

Strategic Systems Project Office
Department of the Navy
ATTN: NSP-272

DEPARTMENT OF THE AIR FORCE

Air Force Flight Dynamics Laboratory
ATTN: FBC
ATTN: FXG

Air Force Geophysics Laboratory
ATTN: LY, C. Touart

Air Force Materials Laboratory
ATTN: MXS
ATTN: MBC
ATTN: LTM
ATTN: MXE
ATTN: MBE

Air Force Rocket Propulsion Laboratory
ATTN: LKCP

Air Force Systems Command
ATTN: DLW

Air Force Weapons Laboratory
ATTN: DYV
ATTN: SUL

Arnold Engineering Development Center
Department of the Air Force
ATTN: Library Documents

Ballistic Missile Office
Air Force Systems Command
ATTN: MNNH
ATTN: MNNR

DEPARTMENT OF THE AIR FORCE (Continued)

Research, Development, & Acq.
Department of the Air Force
ATTN: AFRDQSM
ATTN: AFRDQ

Foreign Technology Division
Air Force Systems Command
ATTN: SDBG

Air Force Systems Command
ATTN: DYSR
ATTN: DYT
ATTN: DYS
7 cy ATTN: DYSE

Strategic Air Command
Department of the Air Force
ATTN: XOBM
ATTN: XPFS

DEPARTMENT OF ENERGY CONTRACTORS

Lawrence Livermore Laboratory
ATTN: Document Control for L-10, H. Kruger
ATTN: Document Control for L-92, C. Taylor

Los Alamos Scientific Laboratory
ATTN: Document Control for J. Taylor

Sandia Laboratories
Livermore Laboratory
ATTN: Document Control for T. Gold

Sandia Laboratories
ATTN: Document Control for D. Rigali
ATTN: Document Control for R. Clem
ATTN: Document Control for A. Chabai

DEPARTMENT OF DEFENSE CONTRACTORS

Acurex Corp.
ATTN: J. Saperstein
ATTN: C. Nardo
ATTN: J. Crenshaw
ATTN: C. Powars

Aerojet Liquid Rocket Co.
ATTN: R. Jenkins

Aeronautical Rsch. Assoc. of Princeton, Inc.
ATTN: C. Donaldson

Aerospace Corp.
ATTN: D. Platus
ATTN: W. Barry

ARO, Inc.
ATTN: J. Adams
ATTN: G. Norfleet

AVCO Research & Systems Group
ATTN: J. Stevens
ATTN: W. Broding
ATTN: A. Pallone
ATTN: V. Dicristina

Boeing Co.
ATTN: B. Lempriere

DEPARTMENT OF DEFENSE CONTRACTORS (Continued)

Calspan Corp.
ATTN: M. Holden

Effects Technology, Inc.
ATTN: R. Wengler

Fiber Materials, Inc.
ATTN: M. Subilia

Ford Aerospace & Communications Corp.
ATTN: A. Demetriades

General Electric Company
ATTN: B. Maguire
ATTN: P. Cline

General Electric Company—TEMPO
ATTN: DASIAC

General Research Corp.
ATTN: R. Rosenthal

Institute for Defense Analyses
ATTN: J. Bengston
ATTN: Classified Library

ION Physics Corp.
ATTN: R. Evans

Kaman Sciences Corp.
ATTN: F. Shelton
ATTN: V. Peckham
ATTN: R. Winnicki

Lockheed Missiles & Space Co., Inc.
ATTN: G. Chrusciel
ATTN: C. Lee
ATTN: R. Au
ATTN: P. Schneider
ATTN: D. Price

Lockheed Missiles & Space Co., Inc.
2 cy ATTN: T. Fortune

Martin Marietta Corp.
ATTN: L. Kinnaird

McDonnell Douglas Corp.
ATTN: H. Hurwicz
ATTN: G. Fitzgerald
ATTN: D. Giedt
ATTN: L. Cohen

National Academy of Sciences
National Materials Advisory Board
ATTN: D. Groves

Pacific-Sierra Research Corp.
ATTN: G. Lang

Physical Sciences, Inc.
ATTN: M. Finson

Physics International Co.
ATTN: J. Shea

Prototype Development Associates, Inc.
ATTN: J. Dunn
3 cy ATTN: C. Thacker

DEPARTMENT OF DEFENSE CONTRACTORS (Continued)

R&D Associates
ATTN: C. MacDonald
ATTN: R. Ross
ATTN: P. Rausch
ATTN: F. Field

Science Applications, Inc.
ATTN: J. Warner

Science Applications, Inc.
ATTN: J. Courtney
ATTN: K. Kratsch
ATTN: L. Dunbar

Science Applications, Inc.
ATTN: A. Martellucci

Southern Research Institute
ATTN: C. Pears

Spectron Development Labs., Inc.
ATTN: T. Lee

DEPARTMENT OF DEFENSE CONTRACTORS (Continued)

SRI International
ATTN: D. Curran
ATTN: G. Abrahamson

Systems, Science & Software, Inc.
ATTN: G. Gurtman

TRW Defense & Space Sys. Group
ATTN: D. Baer
ATTN: R. Myer
ATTN: W. Wood
ATTN: T. Williams
ATTN: I. Alber

TRW Defense & Space Sys. Group
ATTN: E. Wong
ATTN: W. Polich
ATTN: L. Berger
ATTN: E. Allen
ATTN: V. Blankenship
ATTN: W. Grabowski
ATTN: H. Dyner